HHS Public Access

Author manuscript

Nat Immunol. Author manuscript; available in PMC 2019 June 01.

Published in final edited form as:

Nat Immunol. 2018 December ; 19(12): 1403–1414. doi:10.1038/s41590-018-0230-z.

Human retinoic acid-regulated CD161+ regulatory T cells support wound repair in intestinal mucosa

Giovanni AM Povoleri[1,2], **Estefania Nova-Lamperti**[1,2], **Cristiano Scottà**[1,2], **Giorgia Fanelli**[1,2], **Yun-Ching Chen**[3], **Pablo Becker**[1,2], **Dominic Boardman**[1,2], **Benedetta Costantini**[4], **Marco Romano**[1,2], **Polychronis Pavlidis**[1,2], **Reuben McGregor**[1,2], **Eirini Pantazi**[1,2], **Daniel Chauss**[5], **Hong-Wei Sun**[6], **Han-Yu Shih**[7], **David Cousins**[8], **Nichola Cooper**[9], **Nick Powell**[1,2], **Claudia Kemper**[10], **Mehdi Pirooznia**[3], **Arian Laurence**[11], **Shahram Kordasti**[4], **Majid Kazemian**[12], **Giovanna Lombardi**[1,2,*], and **Behdad Afzali**[1,5,13,*,†]

[1]MRC, Centre for Transplantation, King's College London, UK

[2]National Institute for Health Research Biomedical Research Centre at Guy's and St Thomas' NHS Foundation Trust and King's College London, UK

[3]Bioinformatics and Computational Biology Core, National Heart Lung and Blood Institute, National Institutes of Health Bethesda, USA

[4]Department of Haematological Medicine, King's College London, UK

[5]Kidney Diseases Branch, National Institute of Diabetes and Digestive and Kidney Diseases, National Institutes of Health Bethesda, USA

[6]Biodata Mining and Discovery Section, Molecular Immunology and Inflammation Branch, National Institute of Arthritis and Musculoskeletal and Skin Diseases, National Institutes of Health Bethesda, USA

[7]Lymphocyte Cell Biology Section, Molecular Immunology and Inflammation Branch, National Institute of Arthritis and Musculoskeletal and Skin Diseases, National Institutes of Health Bethesda, USA

[8]Department of Infection, Immunity and Inflammation, NIHR Leicester Respiratory Biomedical Research Unit, University of Leicester

[9]Department of Medicine, Imperial College London, London, UK

[10]Complement and Inflammation Research Section, National Heart Lung and Blood Institute, National Institutes of Health Bethesda, USA

[11]Institute of cellular medicine, Newcastle University, Newcastle, UK

[†]Author for correspondence: behdad.afzali@nih.gov; behdad.afzali@kcl.ac.uk.

[*]Equal contribution

Author contributions: G.A.M.P. designed and performed experiments, analyzed data and wrote the manuscript. N.C., N.P. and P.P. provided patient samples and clinical and scientific input. S.K. designed the CyTOF panel, analyzed and interpreted data, provided scientific input and wrote the paper. M.K. analyzed and interpreted genomics data, provided scientific input and wrote the paper. G.L. provided scientific input, supervised the project and wrote the manuscript. B.A. conceptualized the study, supervised the project, analyzed data and wrote the manuscript. E.N-L., C.S., G.F., Y-C.C., P.B., D.B., B.C., M.R., R.M., E.P., D.C., H-W.S., H-Y.S., D.Cousins., C.K., M.P., A.L. performed experiments, analyzed data and/or provided scientific input.

Competing interests:
The authors have no competing interests to declare.

[12]Departments of Biochemistry and Computer Science, Purdue University, West Lafayette, USA

[13]National Heart, Lung and Blood Institute, National Institutes of Health Bethesda, USA

Summary

Repair of tissue damaged during inflammatory processes is key to return of local homeostasis and restoration of epithelial integrity. Here we describe CD161$^+$ regulatory T cells (T_{reg} cells) as a distinct, highly suppressive, population of T_{regs} mediating wound-healing. These T_{regs} were enriched in intestinal lamina propria, particularly in Crohn's disease. CD161$^+$ T_{regs} had an all-trans retinoic acid (ATRA)-regulated gene signature and CD161 expression on T_{regs} was induced by ATRA, which directly regulated the *CD161* gene. CD161 was co-stimulatory and ligation with the T cell receptor induced cytokines that accelerated wound-healing of intestinal epithelial cells. We identified a transcription factor network, including BACH2, RORγt, FOSL2, AP-1 and RUNX1, controlling expression of the wound-healing program and found that a CD161$^+$ T_{reg} signature in Crohn's disease mucosa associated with reduced inflammation. These findings identify CD161$^+$ T_{regs} as a population involved in controlling the balance between inflammation and epithelial barrier healing in the gut.

Introduction

Regulatory T cells (T_{reg} cells) are a non-redundant, suppressive, subset of CD4$^+$ helper T (T_H) cells critical for preventing autoimmunity and ideal for cell-based immunotherapy of autoimmunity and prevention of transplant rejection[1]. T_{reg} cells express the master transcription factor FOXP3, the IL-2 receptor component CD25, the inhibitory co-receptor CTLA4[2] and depend on the transcription factor BACH2[3]. T_{reg} cells are thymically (tT_{reg} cells) and peripherally (pT_{reg} cells) derived and can also be induced *in vitro* (iT_{reg} cells). There are no universally accepted ways to differentiate these populations although expression of Helios, Neuropilin and methylation status of the T_{reg}-specific demethylation region (TSDR) have been proposed[4–8].

Conventional T cells (T_{conv}) express their own master transcription factors; these include T-BET$^+$ T_H1 cells, GATA3$^+$ T_H2 cells and RORγt$^+$ T_H17 cells, respectively[9]. These transcription factors were considered to antagonize T_{reg} development: in mice, induction of high T-bet expression in T_{reg} cells within inflamed bowel drives T_{regs} into a pro-inflammatory phenotype reminiscent of T_h1 cells[10]. This view has been challenged by specific deletions of these factors specifically within Foxp3$^+$ cells of mice[11–14]. For example, T-bet expression within Foxp3$^+$ T_{reg} cells is required for trafficking to and suppression of T_h1-mediated inflammation[13], and Gata3 is required for full T_{reg} function in the gut[14]. These findings support a 'compartmentalized' view of T_{reg} cells, suggesting multiple sub-populations defined by expression of transcription factors associated with T_{conv} lineages and by specialized functions. Indeed, the transcription factor circuitry of T_{reg} cells is complex, with significant interplay between Foxp3 and other lineage-associated transcription factors[15].

In humans, heterogeneous populations of T_{reg} cells have been reported, although typically defined by surface markers (e.g. CD39, HLA-DR and CD45RA[1]) rather than transcription

factors. Whether these sub-populations have the ability to suppress specific parts of the human immune system has yet to be fully elucidated. Conventional methods to delineate T_{reg} subsets are limited by numbers of markers that can be concurrently used and by biased approaches to data analysis (gating of T_{reg} subsets)[16]. This has led to conflicting results, with memory T_{reg} cells reported as both non-suppressive[17] and highly suppressive[18]. By contrast, unbiased multi-dimensional analysis can delineate the most suppressive T_{reg} sub-populations, identify new ones and exclude those less likely to be regulatory[16].

Inflammatory bowel disease (IBD) represents a complex collection of disorders where aberrant mucosal immune system activation, epithelial barrier dysfunction and microbial dysbiosis contribute to chronic inflammation and unregulated local T_H1 and T_H17 responses[19]. Bowel mucosa is a key site for pT_{reg} cell induction from naive $CD4^+$ precursors via instruction from environmental factors, e.g. transforming growth factor (TGF)-β, IL-2 and all-trans retinoic acid (ATRA)[20]. T_{reg} cells mediate dominant tolerance in gut mucosa, preventing or ameliorating murine colitis on adoptive transfer[21]. Conversely, *FOXP3* mutations or disruption of other key T_{reg} cell molecules (e.g. CTLA-4, IL-10R, TGF-β) cause enteropathy in humans and mice[2], demonstrating their key role in preventing gut inflammation. Lamina propria T_{reg} cells increase in number in IBD, but it is unclear why they do not control local inflammation and what function(s) they perform in these diseases[22]. T_{reg} cells can express RORγt together with IL-17A and, in humans, these factors are restricted to a T_{reg} cell subset expressing CD161[23]. CD161 is a C-type lectin-like receptor expressed on human NK cells[24] and various T lymphocyte subsets[25]. $CD161^+$ T_{conv} cells are memory cells acting as T_H17 precursors[26]. The CD161 cognate ligand is lectin-like transcript 1 (LLT1)[27]. Single nucleotide polymorphisms associate with IBD in genome-wide association studies[28], suggesting that the CD161-LLT1 interaction is physiologically important.

Here, we delineate the biological repertoire of $CD161^+$ T_{reg} cells, their role in the immune system and their mechanisms of action. Our data show that $CD161^+$ T_{reg} cells are a highly suppressive, distinct subset of induced T_{reg} cells that accelerate wound healing of colorectal epithelium via production of soluble factors in a BACH2-dependent manner.

Results

CD161-expressing T_{reg} cells are a discrete population with a distinct TCRVβ repertoire

We used an unbiased multi-dimensional analysis pipeline via cytometry by time-of-flight (CyTOF) to identify and study biologically important human T_{reg} sub-populations. Visualized stochastic neighbor embedding (viSNE) was used to create a map of $CD4^+$ T cells from blood and arrange cells along t-distributed stochastic neighbor embedding (t-SNE) axes based on per-cell phenotypic similarity[16,29] (Fig. 1a–b). T_{reg} cells, identified by high expression of CD25 and FOXP3 and low expression of CD127, clustered together and could be resolved into naive and memory populations (Fig. 1a–b). Likewise, T_{conv}, identifiable by low CD25 and FOXP3 and high CD127 expression, clustered together and distinctly from T_{reg} cells (Fig. 1a–b). In this unsupervised analysis, the C-type lectin CD161 was expressed by a sub-population of memory T_{reg} cells ($CD4^+CD25^+CD127^{lo}FOXP3^+CD45RA^-CD45RO^+$) and a group of memory T_{conv} (broadly

$CD4^+CD25^-CD127^+FOXP3^-CD45RA^{lo}CD45RO^+$) (Fig. 1a–b). To identify distinct T cell clusters, we performed a spanning-tree progression analysis of density-normalized events (SPADE)[30] based on t-SNE values. Differential expression of markers within each identified SPADE node was used to further cluster T cells. This analysis resolved $CD4^+$ T cells into 50 sub-populations, grouped into four main populations: naive T_{reg} cells, memory T_{reg} cells, naive T_{conv} and memory T_{conv}, characterized by different expression profiles (Fig. 1c and Supplementary Fig. 1a). CD161-expressing cells represented a distinct sub-population of memory T_{reg} cells and several sub-populations of memory T_{conv}, which were all distinct from T_{reg} cells (Fig. 1c). To further distinguish T_{reg} cells from T_{conv}, we performed similar analysis of transcriptomes by single-cell RNA-seq using $CD4^+CD25^+$ cells as input (Supplementary Figs. 1b–e). This pipeline resolved cells into 9 clusters, of which two were T_{reg} cells (clusters 0 and 3), five were T_{conv} (clusters 1, 2, 4, 5 and 6) and two were probably T_{reg} cells although too small in number to sub-categorize (clusters 7 and 8) (Supplementary Figs. 1b–e). The two T_{reg} clusters (clusters 0 and 3) were clearly separate from the T_{conv} clusters and one of them (cluster 3) expressed *KLRB1*, the gene encoding CD161 (Supplementary Figs. 1b–e). Consistent with CyTOF, expression of *KLRB1* in $CD161^+$ T_{regs} was lower than the $CD161^+$ T_{conv} sub-population. A heatmap of T_{reg} markers (*IL2RA*, *IL7R*, *FOXP3*), *KLRB1* and naive or memory markers (*CD62L* and *CCR7*) confirmed clustering of the $CD161^+$ T_{reg} cells (cluster 3) independently from T_{conv} cells (Supplementary Fig. 1e) and was similar to heatmaps constructed from protein expression by CyTOF (Supplementary Fig. 1f). A similar unsupervised pipeline applied to $CD4^+$ T cells flow-stained with just 5 markers, CD4, CD25, CD127, CD45RA and CD161 produced similar viSNE and SPADE plots to CyTOF (Supplementary Fig. 1g–h) and could be used to flow-sort peripheral blood T_{reg} sub-populations for further analysis (Supplementary Figs. 1i–j). Henceforth, these T_{reg} cells are referred to as '$CD161^+$ T_{reg} cells' ($CD4^+CD25^{hi}CD127^{lo}CD45RA^-CD161^+$; denoted in purple), 'naive T_{reg} cells' ($CD4^+CD25^{hi}CD127^{lo}CD45RA^+CD161^-$; denoted in orange) and $CD161^-$ memory T_{reg} cells, abbreviated to 'memory T_{reg} cells' ($CD4^+CD25^{hi}CD127^{lo}CD45RA^-CD161^-$; denoted in yellow).

T cell CD161 expression is associated with a restricted range of T cell receptors (TCRs): Vα7.2 in mucosal-associated invariant T (MAIT) cells[25] and invariant Vα24-Jα18 in iNKT cells[31]. Neither TCR was significantly enriched in $CD161^+$ T_{reg} cells (Supplementary Fig. 1k). To determine clonality of $CD161^+$ T_{reg} cells and their relationship to other T_{reg} cells and T_{conv}, we *TCRVB* sequenced the three T_{reg} cells populations, as well as T_{conv} (defined as $CD4^+CD25^-CD127^+$) and $CD161^+$ T_{conv} (defined as $CD4^+CD25^-CD127^+CD45RO^+CD161^+$) as controls. Among the TCRBV families, the three highest contributors to the total TCR repertoire (BV05, BV06 and BV07) and one of the lower contributors (BV19) were chosen to represent variability of the cellular repertoire by spectratyping. $CD161^+$ T_{reg} cells were polyclonal, had normally distributed CDR3 length in the different TCRBV families (Fig. 1d) and similar contribution to the overall TCR repertoire compared with other T cell subsets (Supplementary Fig. 1l). We asked whether the TCR repertoire of $CD161^+$ T_{reg} cells overlapped with either the T_{reg} or T_{conv} populations and found limited clonality shared between the different subsets; in particular, $CD161^+$ T_{reg} cells shared only 4.5% and 4.8% of TCR sequences with Memory T_{reg} cells and $CD161^+$ T_{conv} cells, respectively

(Supplementary Fig. 1m). We calculated the Morisita-Horn similarity index to measure TCR composition overlap between the different T cell populations[32] - this index ranges between 0 (minimal similarity) and 1 (maximal similarity). Limited TCR repertoire overlap existed between any of the populations other than between CD161$^+$ T_{conv} and T_{conv} (a value of 0.413) (Fig. 1e). Hierarchical clustering, based on the Morisita-Horn similarity index, indicated two subdivisions, separating the two T_{conv} populations from all three T_{reg} populations; moreover, CD161$^+$ T_{reg} cells clustered with memory T_{reg} cells within the regulatory T cell main branch (Fig. 1f). These data indicate that CD161$^+$ T_{reg} cells have distinct TCR repertoires from other T_{reg} cells and do not represent a clonal expansion from a T_{conv} population.

CD161$^+$ T_{reg} cells share features with both CD161$^+$ T_{conv} and classical T_{reg} cells

To identify similarities and differences between the 3 sub-populations, we compared their transcriptomes using microarray and Gene Set Enrichment Analysis (GSEA) (Supplementary Fig. 2a–d). Despite CD161$^+$ T_{reg} cells being a sub-population of memory T_{reg} cells, there were 549 genes differentially expressed when comparing CD161$^+$ to memory T_{reg} cells (Fig. 2a, Supplementary Fig. 2b–d and Supplementary Table 1). CD161$^+$ T_{reg} cells were enriched in genes expressed by other CD161$^+$ cells[25] and also expressed the core transcriptional profile of T_{reg} cells[33] (Fig. 2b–c and Supplementary Fig. 2e–f). This data suggested that, in addition to core T_{reg} genes they express a range of other transcripts related to CD161 induction or signaling.

All three T_{reg} populations had similar FOXP3 protein expression (Fig. 2d). We measured the methylation status of the *FOXP3* TSDR and two other key T_{reg}-associated genes, *IL2RA* and *CTLA4*, in the three T_{reg} populations and, for comparison, T_{conv} (Supplementary Fig. 2g). Methylation at *IL2RA* and *CTLA4* loci were similar between the three T_{reg} populations but distinct from the more highly methylated T_{conv} (Fig. 2e and Supplementary Fig. 2h). At the *FOXP3* TSDR we noted CD161$^+$ T_{reg} cells to have methylation intermediate (55%) between naive (25%) or memory (28%) T_{reg} cells and T_{conv} (88%) (Fig. 2e and Supplementary Fig. 2h), a figure similar to that seen in studies that compared Helios$^+$ T_{reg} cells with Helios$^-$ T_{reg} cells in humans[34]. In summary, CD161$^+$ T_{reg} cells express the T_{reg} master transcription factor FOXP3, the same surface markers as T_{reg} cells and the T_{reg} gene transcription profile. Their methylation pattern at key gene loci are similar to other T_{reg} cells, albeit with intermediate TSDR methylation.

ATRA directly regulates CD161 expression

Long-term *in vitro* culture of T_{reg} cells with ATRA supports persistence of cells expressing CD161[35]. CD161$^+$ T_{reg} cells were enriched in ATRA-regulated genes compared to memory T_{reg} cells (Fig. 3a) by GSEA, including two gut homing markers, *CCR9* and *ITGA4*, which are classical ATRA-regulated genes (Fig. 3a and Supplementary Fig. 3a); CCR9 was confirmed at the protein level by flow cytometry (Supplementary Fig. 3b). Activation of freshly-isolated T_{reg} cells with ATRA induced expression of both CCR9 and CD161 (Fig. 3b). Since T_{reg} cells interact with dendritic cells (DCs) in the gut, we determined if mature DCs generate ATRA via a functional assay for the key enzyme aldehyde dehydrogenase (ALDH). Lipopolysaccharide (LPS)-matured DCs expressed substantial ALDH enzyme

(Fig. 3c) together with lectin like transcript 1 (LLT1), the natural ligand for CD161 (data not shown)[27]. In the absence of DCs, T_{reg} cells lost CD161 expression; whereas co-culture of freshly-isolated T_{reg} cells with DCs induced CD161. Addition of BMS493, a pan-retinoic acid receptor (RAR) inverse agonist blocked CD161 expression in a dose-dependent manner (Fig. 3d and Supplementary Fig. 3c). To see whether ATRA directly regulates CD161, we scanned the *KLRB1*, which encodes CD161, and *CCR9* gene loci (as control) for retinoic acid receptor alpha (RARA) DNA binding motifs (Supplementary Fig. 3d). One potential RARA site in *KLRB1* and multiple sites in *CCR9* were identified (Supplementary Fig. 3e). By *RARA* ChIP-qPCR we found that ATRA enhanced RARA binding at both loci in T cells, evident as significant increment in percentage of input for both *KLRB1* and *CCR9* target sequences after culture with ATRA, compared to untreated cells (Fig. 3e). Collectively, these data indicate that ATRA can induce CD161 expression on T_{reg} cells.

CD161$^+$ T_{reg} cells are a highly suppressive T_{reg} population

We next tested the ability of CD161$^+$ T_{reg} cells to suppress T_{conv} proliferation *ex vivo* by measuring the ratio of T_{reg} cells to T_{conv} required to suppress proliferation by 50% (IC_{50}) for each population[36] (Fig. 4a–b and Supplementary Fig. 4a–b). CD161$^+$ T_{reg} cells had a lower mean IC_{50} compared to memory T_{reg} cells, whereas naive T_{reg} cells did not reach 50% suppression *ex vivo* (and therefore IC_{50} could not be calculated) (Fig. 4b and Supplementary Fig. 4b). CD161$^+$ T_{reg} cells remained stably regulatory even after *in vitro* proliferation for two weeks (Supplementary Fig. 4c). Separation of T_{reg} cells from target cells by a transwell abrogated the majority of the suppressive function of CD161$^+$ T_{reg} cells (Supplementary Fig. 4d), suggesting contact-dependent effects and consistent with other T_{reg} populations[37]. The presence of anti-CD161, anti-PD-L1, anti-TGFβRII or anti-IL-10R antibodies caused no significant impairment of CD161$^+$ T_{reg} suppressive function, indicating that suppressive function is likely not due to a single factor (Supplementary Fig. 4e). Furthermore, suppression assays under T_H1 and T_H17 skewing conditions did not impair regulatory function in CD161$^+$ T_{reg} cells (Supplementary Fig. 2f). CD161 is found on NK cells[24] and cytotoxicity is a suppressive mechanism of some T_{reg} cells[38]. However, we found neither perforin nor granzyme (A or B) in any of the T_{reg} populations (Supplementary Fig. 4g) and no evidence of T_{conv} cytolysis after co-culture with CD161$^+$ T_{reg} cells (data not shown).

The mouse CD161 ortholog is not expressed on T cells (Supplementary Table 2). To confirm suppressive ability of CD161$^+$ T_{reg} cells *in vivo*, we used a humanized mouse model of severe xeno-graft versus host disease (GvHD) in NOD-SCID-*Il2rg*$^{-/-}$ (NSG) mice by injecting CD25-depleted human peripheral blood mononuclear cells (PBMC) with or without *in vitro*-expanded memory or CD161$^+$ T_{reg} cells. Mice receiving either memory or CD161$^+$ T_{reg} cells were protected from xeno-GvHD, surviving significantly longer than mice injected with PBMC alone and had significant reduction in clinical disease scores (Fig. 4c). Thus, CD161$^+$ T_{reg} cells had comparable suppressive activity to traditional T_{reg} cells *in vivo*. These data indicate that CD161$^+$ T_{reg} cells are highly regulatory both *in vitro* and *in vivo*.

CD161 ligation stimulates cytokine production in CD161$^+$ T$_{reg}$ cells

We next investigated the specific effects of TCR triggering by examining transcriptomes of T$_{reg}$ cells stimulated with anti-CD3+CD28 for 4 hours. Approximately 1500 transcripts showed changes from baseline in CD161$^+$ T$_{reg}$ cells (Fig. 5a and Supplementary Fig. 5a–b). Although a core set of transcripts, including *KLRB1*, *RORC* and *CCR9* differed between CD161$^+$ and memory T$_{reg}$ cells both before and after these cells were activated, there was little overlap (Fig. 5b–c). Of note, a number of cytokine genes, including *IL10*, *IL17A*, *IL17F* and *IL21* (Fig. 5c), were enriched in CD161$^+$ T$_{reg}$ cells (Supplementary Fig. 5b). We confirmed preferential accumulation of IL-10, IL-17A, IL-22 and IL-4, but not IFN-γ, in three-day supernatants of αCD3+CD28-activated CD161$^+$ T$_{reg}$ cells (Fig. 5d).

CD161 in T$_{conv}$ is a marker of T$_H$17 cells. Furthermore, CD161$^+$ T$_{reg}$ cells expressed RORC, the key transcription factor of T$_H$17 cells, along with IL-17 itself. We next determined whether IL-17 production was compatible with suppressive function in CD161$^+$ T$_{reg}$ cells, by isolating IL-17$^+$CD161$^+$ and IL-17$^-$CD161$^+$ T$_{reg}$ cells using an IL-17 capture assay (Supplementary Fig. 5c–d) and testing their respective suppressive functions. IL-17$^+$CD161$^+$ T$_{reg}$ cells remained highly suppressive despite producing IL-17 (Fig. 5e).

CD161 does not have classical immunoreceptor tyrosine-based activation or immunoreceptor tyrosine-based inhibitory domains but its ligation can have both activating and inhibitory functions, depending on cell type[25,39]. To assess the function of CD161 in T$_{reg}$ cells, we stimulated cells with anti-CD3+anti-CD28 magnetic beads additionally coated with anti-CD161 or an IgG2 isotype. After three days of culture CD161 cross-linking significantly enhanced cytokine production from CD161$^+$ T$_{reg}$ cells (Fig. 5f), indicating that CD161 acts as a co-stimulatory molecule in CD161$^+$ T$_{reg}$ cells. Thus, CD161$^+$ T$_{reg}$ cells are a cytokine producing population of T$_{reg}$ cell, CD161 co-ligation is co-stimulatory to this process and IL-17 production is compatible with suppressive function.

Genome-wide chromatin landscapes define regulatory circuitry in CD161$^+$ T$_{reg}$ cells

We next examined global chromatin landscapes of naive, memory and CD161$^+$ T$_{reg}$ cells directly *ex vivo* using high-throughput sequencing ATAC-seq, hypothesizing that these dictate differences in biological function. Open chromatin regions (OCRs) surrounding the signature T$_{reg}$-associated genes, notably *FOXP3*, *CTLA4* and *IL2RA* were not significantly different between the three populations (Supplementary Fig. 6a). We focused on ~1300 OCRs that have consistent patterns among all three biological replicates but differ among the three T$_{reg}$ populations. These regions were in three clusters: those specific to naive T$_{reg}$ cells (25% of total), specific to CD161$^+$ T$_{reg}$ cells (39% of the total) and those shared between CD161$^+$ and memory T$_{reg}$ cells (37% of the total) (Fig. 6a–b and Supplementary Table 3). Examples of genes with OCRs specific to CD161$^+$ T$_{reg}$ cells included cytokines, such as *IL17A*, transcription factors, such as *PRDM1* and *MAF*, and chemokine receptors, including *CCR9* (Supplementary Table 3). The genomic distributions of OCRs were similar in the three clusters, with the majority within intronic and intergenic regions (Supplementary Fig. 6b).

To determine potential transcription factors targeting distinct T_{reg} regulomes, we searched for enrichment of known motifs above background within OCR clusters using HOMER (Fig. 6c and Supplementary Fig. 6c). CD161$^+$-specific OCRs were enriched for motifs of RORγt, RUNX, AP-1 family (e.g. BATF, FOSL2), and Cap'n'collar (CNC) family members that include BACH2 (Fig. 6c and Supplementary Fig. 6c). We performed GSEA for genes regulated by BACH2, RORγt, BATF, FOSL2 and RUNX1. CD161$^+$ T_{reg} cells were enriched for BACH2, RORγt, FOSL2 and RUNX1 regulated genes, compared to memory T_{reg} cells (Fig. 6d). Approximately 40% of the 549 genes differentially expressed between CD161$^+$ and memory T_{reg} cells could be attributed to regulation by *Bach2*, *Runx1*, *Rorc*, *Fosl2* and *Batf* in mice using knockout models[3,40,41], with BACH2 responsible for the majority of the transcriptional differences (Fig. 6e). Expression of BACH2 itself was significantly reduced and RORC significantly elevated in freshly isolated CD161$^+$ T_{reg} cells compared to other T_{reg} populations (Supplementary Fig. 6d), suggesting that altered expression of these transcription factors could explain some of the transcriptional differences seen in their targets. CD4$^+$ T cells from a patient heterozygous for a BACH2^{L24P} mutation rendering her BACH2 haploinsufficient[42] showed over-representation of the CD161$^+$ T_{reg} subset relative to controls (Fig. 6f), confirming that low BACH2 expression is important for development and/or persistence of these cells. An integrated network was constructed based on these effects to illustrate the transcriptional circuitry (Supplementary Fig. 6e). Genes controlled solely by BACH2 regulated cell division, whereas genes co-regulated by BACH2 and the other transcription factors in this model were especially involved in wound healing (Fig. 6f). These data point to distinct regulomes in CD161$^+$ T_{reg} cells imparting novel functions including wound-healing.

CD161$^+$ T_{reg} cells are enriched in IBD, enhance wound healing and associate with reduced inflammation

We confirmed by GSEA that activated CD161$^+$ T_{reg} cells were enriched for wound healing genes (e.g. *PDGFA* and *CFS2*), including soluble mediators (e.g. *IL17A* and *IL22*), compared to other T_{reg} populations (Supplementary Fig. 7a–b). Since CD161$^+$ T_{reg} cells expressed *CCR9* and *ITGA4* (Fig. 3a and Supplementary Fig. 3a–b), we determined if they were enriched in the bowel during inflammation by comparing T_{reg} populations in matched peripheral blood to colonic biopsies of healthy individuals and those with Crohn's disease (CD). There was mild enrichment of naive and memory T_{reg} cells in colonic mucosa compared to blood. By contrast, there was a significant enrichment of CD161$^+$ T_{reg} cells in healthy colons, which was even more pronounced in patients with CD (Fig. 7a). LLT1, the CD161 ligand, is expressed in inflamed areas[27], which we speculated would drive cytokine expression in CD161$^+$ T_{reg} cells. We therefore tested the effect of CD161$^+$ T_{reg} supernatants on wound healing using a human epithelial colorectal adenocarcinoma cell line (Caco-2 cells) to approximate bowel epithelium. Supernatants from activated CD161$^+$ T_{reg} cells increased and accelerated closure of the wound by almost two-fold compared to supernatant from memory T_{reg} cells or medium alone (Fig. 7b–c, Supplementary Fig. 7c and Supplementary Movies 1–3). Neutralization of IL-17 alone, IL17 together with IL-22, IL-4 or IL-10 impeded the wound healing capacity of supernatants of activated CD161$^+$ T_{reg} cells, implicating these cytokines as mediators of wound healing (Fig. 7d). Over-expression of BACH2 by lentiviral delivery in CD161$^+$ T_{reg} cells significantly inhibited production of

IL-17 and IL-4, with a similar but not significant trend in IL-22 and IL-10 (Fig. 7e and Supplementary Fig. 7d), supporting the notion that the wound healing program of CD161$^+$ T_{reg} cells is dependent on reduced expression of the repressive BACH2 transcription factor in these cells.

The suppressive function of CD161$^+$ T_{reg} cells and their ability to accelerate wound healing suggested that they might be beneficial in IBD. To explore this possibility, we examined RNA-seq from a large dataset of patients with CD (GSE57945) for expression of *KLRB1*, which encodes CD161. *KLRB1* correlated negatively with 15 genes previously shown to be upregulated in inflamed, compared to uninflamed, CD mucosa[43] (Fig. 7f). Of these, *CXCL1*, a clinical biomarker of CD, was significantly more highly expressed in inflamed versus uninflamed CD mucosa, while *KLRB1* expression was significantly higher in uninflamed CD mucosa (Fig. 7g). *KLRB1* is expressed on both T_{reg} cells, which are IL-7R^{lo}, and T_H17 cells, that are IL-7R^{hi}. We used GSE57945 as a training dataset to test the performance of *KLRB1*, *IL7R* and *KLRB1*/*IL7R* ratio to distinguish inflamed from uninflamed CD. The receiver operating characteristic (ROC) curve for *KLRB1*/*IL7R* was highly significant (AUC=0.77; p-value<0.0001) and performed well in comparison with *CXCL1*, slightly better than *KLRB1* and substantially better than *IL7R* alone (Fig. 7h) when predicting inflamed versus uninflamed mucosa. We used two additional transcriptome datasets from CD mucosa as validation datasets. In all cases the *KLRB1*/*IL7R* predictor was higher in uninflamed CD mucosa (Fig. 7i) and distinguished inflamed from uninflamed mucosa (AUC range 0.63 to 0.79; Fig. 7j), suggesting that tissue infiltration with CD161$^+$ T_{reg} cells is associated with lower inflammation in CD. These data suggest that CD161$^+$ T_{reg} cells are enriched in colonic mucosa, particularly in IBD, where they suppress inflammation and produce soluble factors that accelerate epithelial barrier healing, having a beneficial effect on outcomes.

Discussion

Understanding biologically important and clinically relevant T_{reg} populations is key to elucidating disease mechanisms and tailoring immunotherapy. We delineated CD161$^+$ T_{reg} cells in humans, showing them to be a distinct, highly suppressive, *bona fide* retinoic-acid dependent sub-population enriched in lamina propria and associating with regions that have lower inflammation in CD. We show that they can enhance wound healing through soluble mediators and that transcriptional control involves a transcription factor network in which BACH2, RORγt, RUNX1, FOSL2 and BATF, all play a role. We show phenotypic distinction of CD161$^+$ T_{regs} from T_{conv}, including a unique TCR repertoire that is different from T_{conv} and T_H17 cells. Thus, it is highly unlikely that they are contaminating T_{conv}. We conclude that they are a distinct sub-population of T_{reg} cells with stable regulatory function.

CD161$^+$ T_{reg} cells are either induced to develop or specialize in the periphery, consistent with absence of CD161$^+$ T_{reg} cells in cord blood[23] and thymus (our unpublished observations) and relatively small circulating numbers. Murine RORγt$^+$ T_{reg} cells can either develop in the colon from naive CD4$^+$ T cells by local microbiota to suppress intestinal inflammation, although these cells do not produce IL-17[44], or from thymic T_{reg} émigrés following immunization[45]. We identified that human CD161$^+$ T_{reg} cells have a retinoic acid-

regulated gene signature and that retinoic acid directly regulates *KLRB1*, the gene encoding CD161. Since bowel is rich in retinoic acid, an area for T_{reg} generation and since $CD161^+$ T_{reg} cells expressed CCR9, a gut-homing chemokine receptor, it was unsurprising that the lamina propria was enriched in $CD161^+$ T_{reg} cells, particularly in IBD. This is consistent with inflamed bowel as an enrichment site for $FOXP3^+IL\text{-}17^+$ T cells[46]. Thus, $CD161^+$ T_{reg} cells appear to be either induced or migrate to lamina propria.

Some open chromatin regions (OCRs) were broadly accessible in all three T_{reg} populations we studied, including T_{reg} lineage-associated loci, e.g. *FOXP3*, *CTLA4* and *IL2RA*, consistent with similar protein expression in all the subsets. The regulomes of $CD161^+$ T_{reg} cells differed from memory T_{reg} cells by only ~500 OCRs, congruous with relatively small transcriptional differences between them. The transcription factor circuitry explaining these differences was dominated by BACH2, which was itself expressed at lower level in $CD161^+$ *versus* memory T_{reg} cells. The importance of low BACH2 expression for development and/or persistence of these T_{reg} cells was demonstrated by excess of $CD161^+$ T_{regs} in a patient with genetic BACH2 haploinsufficiency. As BACH2 restricts T cell effector programs[3], it is unsurprising that de-repression by BACH2 imparts functional properties to T_{reg} cells resembling T_{conv} cells, notably cytokine production, without loss of suppressive phenotype. This is supported by significantly diminished cytokine production with BACH2 over-expression in these T_{regs}. Notably, *CCR9* is a classic BACH2-repressed gene[3] and one of the most differentially expressed genes in $CD161^+$ T_{reg} cells.

The CD161 ligand, LLT1, is expressed on activated DCs and in actively inflamed areas[27], hence cross-linking of CD161 is likely in inflamed areas of bowel. Indeed, single nucleotide polymorphisms in LLT1 associate with IBD[28]. CD161 cross-linking synergized with anti-CD3+CD28-mediated signals to induce cytokine secretion in $CD161^+$ T_{regs}, in agreement with CD161 stimulating proliferation and cytokine secretion on other T lymphocytes[25] but contrasting with the inhibitory effect of CD161 ligation on NK cells[39]. This suggests that signals transduced by CD161 has cell-type and possibly context-dependent effects.

Although the association between CD161 and T_H17 programs in T_{conv} is known, it was unexpected that transcriptomes of activated $CD161^+$ T_{reg} cells encode complex cytokine cocktails. Since IL-17 can be pro-inflammatory and is associated with autoimmunity, it was possible that IL-17 expression could have denoted a pro-inflammatory function. Indeed, in mice $ROR\gamma t^+$ T_{reg} cells can promote autoimmunity and cancer[47,48]. Our data, however, indicate that actively IL-17-producing T_{reg} cells remain highly suppressive and we found no evidence that $CD161^+$ T_{reg} cells are a transitional or unstable population, consistent with mouse models where adoptive transfer of $IL\text{-}17^+Foxp3^+ROR\gamma t^+$ T cells supports stable suppressive effects on gut inflammation[49]. The cytokine profile of $CD161^+$ T_{reg} cells could denote additional functions, in addition to cellular suppression, such as a potential role in wound healing[50]. In fact, several cytokines produced by $CD161^+$ T_{reg} cells, such as IL-17 and IL-22, have established wound healing roles, especially in the gut. IL-17 can promote epithelial repair and protect from excessive inflammation in colitis models[51]. Indeed, IL-17 blockade exacerbates human and murine colitis[52]. IL-22 also induces intestinal epithelial regeneration and protects from GvHD[53], as well as dampening inflammation in models of

IBD[54]. In conclusion, these data support the notion that enhancing CD161$^+$ T_{reg} cells at the site of inflammation, for example by cell therapy, might prove beneficial in IBD.

Online methods

T cell separation, sorting, and flow cytometry

Human PBMCs (peripheral blood mononuclear cells) and T cells subsets were purified from either anonymized leukodepletion cones (Blood Transfusion Service, NHS Blood and Transplantation, Tooting, London, UK) or fresh blood of healthy volunteers. Human studies were conducted in accordance with the Declaration of Helsinki and approved by the Institutional Review Board of Guy's Hospital (reference 09/H0707/86). Informed consent was obtained from all healthy donors. T_{reg} cells were isolated by initially enriching with CD4$^+$ T Cell Isolation Kit II (Miltenyi Biotec), cells were subsequently stained with mouse anti human CD4 (OKT4), CD127 (eBioRDR5), CD45RA (HI100, all from eBiosciences) and CD25 in PE (both 2A3 and M-A251) and CD161 (DX12, all from BD Biosciences); PE-labelled cells were then captured using anti-PE MicroBeads (Miltenyi Biotec) to enrich for T_{reg} cells, pre-sorting. Cells were FACS sorted for surface markers to separate naive (CD4$^+$CD25^{hi}CD127^{lo}CD45RA$^+$CD161$^-$), memory (CD4$^+$CD25^{hi}CD127^{lo}CD45RA$^-$CD161$^-$), and CD161$^+$ (CD4$^+$CD25^{hi}CD127^{lo}CD45RA$^-$CD161$^+$) T_{reg} cells. Sorting of naive T_{conv} (CD4$^+$CD25$^-$CD45RA$^+$CD161$^-$), total T_{conv} (CD4$^+$CD25$^-$) and T_H17 (CD4$^+$CD25$^-$CD45RA$^-$CD161$^+$) cells was performed using the same panel. Intracellular staining for FOXP3 (PCH101, eBioscience) was carried out using the Foxp3 / Transcription Factor Staining Buffer Set Kit (eBioscience) according to manufacturer's instructions. For intracellular staining of cytokines and transcription factors cells were activated for 4 hours with PMA (50 ng/mL) and ionomycin (1 mM, both from Sigma) with the addition of Brefeldin A (3 μg/mL; eBioscience) before staining. Additional staining of T_{reg} cells were further stained for invariant chains TCRVα24-Jα18 (6B11) and TCR Vα7.2 (3C10, both from Biolegend), perforin (dG9, eBioscience), granzyme A (GB11, Biolegend) and granzyme B (CB9, Biolegend) using appropriate flurochrome-conjugated antibodies. Flow cytometry data were acquired on an LSR Fortessa (BD) and subsequenrly analyzed using FlowJo version 10.1 (TreeStar Inc.).

Mass Cytometry (CyTOF)

2×10^6 CD4$^+$CD127^{lo} cells were isolated using RosetteSep™ Human CD4$^+$CD127^{low} T Cell Enrichment Cocktail (STEMCELL Technologies) before extracellular and intracellular staining with metal conjugated antibodies. For full list of both antibody panels refer to Supplementary Table 4. CyTOF-2 mass cytometer (Fluidigm) was used for data acquisition and beads (Ce140) were used for normalization [29]. 320,000 cells were proportionally sampled from all individuals to perform automated clustering. Data were initially processed and analysed using Cytobank [29]; CD4 sample "cleanup" was performed by gating on intact (191Ir$^+$ DNA stain), no beads (Ce140$^-$), live (103Rh$^-$), no B cells CD19$^-$CD20$^-$ (Nd142), no neutrophils CD15$^-$ CD123$^-$ (Eu151), CD34$^-$ (Er166), CD45$^+$(Y89), CD3$^+$ (Sm154) and CD4$^+$ (Nd145) T cells. Mass-cytometry complex data was analysed using viSNE, in combination with SPADE, to identify distinct subpopulations [30,55] using the following parameters: CCR6 (141Pr), CD45RA (143Nd), CCR4 (149Sm), CD161 (150Nd), CD103

(152Sm), CD62L (153Eu) Helios (156Gd), CCR7 (159Tb), Tbet (160Gd), CD95 (161Dy), CXCR3 (163Dy), CD45RO (164Dy), GATA3 (167Er), CCR9 (168Er), CD25 (169Tm), Foxp3 (171Yb), CXCR4 (173Yb), HLA-DR (174Yb), CD127 (176Yb). viSNE and SPADE plots were generated using Cytobank Inc. (CA, USA). When indicated in the figure legend, figures were overlaid for demonstration purpose.

T cell culture

Unless indicated otherwise, cells were cultured in X-Vivo 15 with Gentamycin and PR (Lonza) supplemented with Penicillin-Streptomycin Glutamine (PSG, Thermo Fisher) and 5% human AB serum (Biosera), henceforth shortened to X-Vivo 5% HS; cells were then seeded at 10^6cell/ml.

For the evaluation of the effect of ATRA on CD161 expression, 250,000 total T_{reg} cells were isolated and stimulated for 48h with 1:1 ratio of αCD3/CD28 Dynabeads in X-Vivo 5% HS supplemented with 100IU/ml of IL-2 (Proleukin, Novartis), in the presence of 0, 0.02, 0.2 or 2μM ATRA (Sigma-Aldrich); cells were then stained for CD4, CD161 and CCR9 and the effects of ATRA on expression of CD161 (stained with anrtibody clone DX12 from BD) and CCR9 (stained with antibody clone L053E8 from Biolegend) was evaluated by flow cytometry.

For T_{reg} cell expansion to facilitate *in vivo* models sorted memory and $CD161^+$ T_{reg} cells were cultured in X-Vivo 5% HS supplemented with 1,000 IU/ml IL-2 and stimulated with anti-CD3+CD28 Dynabeads at a 1:1 ratio for 2–3 rounds of expansion of 10–14 days each. Beads were removed by magnetic adherence following each round of stimulation and fresh anti-CD3+CD28 Dynabeads (1:1 ratio) added. After the last round of expansion, beads were removed and the cells were rested for 2 days before injection. Cell viability was close to 100% prior to each *in vivo* experiment.

To evaluate the effects of CD161 crosslinking on cytokine production, $CD161^+$ T_{reg} cells were cultured for 3 days in X-Vivo 5% HS, supplemented with 100 IU/ml IL-2 and stimulated 1:1 with microbeads from the T cell activation/expansion kit (Miltenyi Biotec) loaded with anti-CD3 and anti-CD28 following manufacturer's instructions with the addition of anti-CD161 (191B8, MiItenyi) or IgG2a (eBM2a eBioscience).

T_{reg} cell suppression assay

Cryopreserved T_{conv} cells ($CD4^+CD25^-$) were used as target cells throughout. These were isolated by negative selection of $CD4^+$ T cells followed by positive selection of $CD25^+$ T cells using miniMACS $CD4^+CD25^+$ T Regulatory Cell Isolation Kit (Miltenyi Biotec, UK) according to manufacturers' instructions. T_{conv} cells were obtained from the $CD25^-$ negative fraction. Cryopreserved T_{conv} were thawed and labelled with either 2.5μM Carboxyfluorescein diacetate, sucinnimydil ester (CFSE) (Molecular Probes, USA) or 1μM CellTrace Violet (CTV) (Molecular Probes, USA) according to manufacturers' instructions. T_{conv} cell viability was routinely greater than 95% prior to suppression assay. Suppression assays were conducted in X-Vivo 5% HS and U-bottom 96-well plates incubated at 37°C, 5% CO_2 for 5 days, at constant T_{conv} cell number (10^5 cells) and T_{reg} cells :T_{conv} ratio of 1:1 or 1:2, as indicated. Where indicated, T_{reg} cell numbers were titrated to result in a T_{reg}

cells : T_{conv} ratio of 1:1 to 1:32 ratio. Cells were stimulated with αCD3/CD28 Dynabeads (bead:cell ratio of 1:40) and CFSE/CTV dilution was assessed by flow cytometry on day 5. Percentage of suppression and IC_{50} were calculated as previously described[36]. Where indicated, T_{reg} cell suppression was also evaluated in the presence of either 10μg/ml anti-CD161 (BD Pharmingen), 10μg/ml anti-PDL-1 (eBioscience), 10μg/ml anti-IL-10R (Sigma), 1μg/ml αTGFBRII (R&D) or in the presence of T_H1 (40ng/mL IL-12 (Biolegend) and 5μg/mL anti-IL-4 (R&D)) or T_H17 (40ng/mL IL-1β (R&D) and IL-6, 10ng/mL TGF-β1 (both from Biolegend), 50ng/mL IL-23 and 5μg/mL anti-IL-4 and anti-IFNg, all from R&D) skewing conditions.

For transwell suppression assay the HTS Transwell-96 Permeable Support with a 0.4μm Pore Polycarbonate Membrane system (Corning) was used. Suppression was tested at a 1:1 T_{reg} cells : T_{conv} ratio and T_{conv} were seeded in the lower compartment of the transwell plate, while T_{reg} cells were seeded on to the upper compartment. Cells in both the upper and lower chambers were stimulated with anti-CD3+CD28 Dynabeads (bead:cell ratio of 1:40). As reference of standard suppression, T_{reg} cells and T_{conv} were also co-seeded in the lower compartment.

Gene expression analysis

200,000 naive, memory and $CD161^+$ T_{reg} cells were either sorted from fresh blood directly into Trizol LS (Ambion) for baseline genetic profile or cells were polyclonally activated post-sorting for 4h with Dynabeads Human T-Activator CD3/CD28 (ratio 1:1) and then lyzed in Trizol LS. RNA was isolated using RNeasy mini kit (QIAGEN) and Ovation PicoSL WTA System V2 (NuGEN Technologies) was used for reverse transcription and cDNA amplification steps. Fragmentation and labelling was performed using the Encore Biotin Module (NuGEN Technologies); all kits were employed following manufacturer's instructions. Samples were run on GeneChip® Human Gene 1.0 ST Array (Affymetrix Ltd). Data analysis was performed using Partek Genomic SuiteTM (Partek Incorporated). Thresholds for significance were set at 1.5-fold difference at $p<0.05$ for freshly isolated cells and 2-fold difference at $p<0.05$ for *in vitro* activated cells.

Gene set enrichment analysis (GSEA) was performed using GSEA version 2.2.2 [56]. Datasets used for GSEA are shown in Supplementary table 1. Core human T_{reg} cell genes were sourced from [33]; genes associated with $CD161^+$ cells were obtained from[25]. The ATRA-regulated gene list was generated by microarray from human T_{reg} cells treated, or not, with ATRA (Scottà *et al.* unpublished data). Genes regulated by RORC, BATF, and FOSL2 were curated from comparison of wild type and single gene knock-out T_h17 cells from [41](GSE40918), RUNX1 from wild type and *Cbfbeta* knockout T_{reg} cells[40] (GPL1261) and BACH2 from wild type and *Bach2* knockout T_{reg} cells[3] (GSE45975), all at a significance threshold of 1.5-fold change and $p<0.05$. Mouse gene symbols were converted to human homologs using the BioMart data-mining tool in ensemble: http://www.ensembl.org/biomart/martview. General wound healing associated genes were curated from published gene lists [57–59], the "resolve wound healing and fibrosis-related genes" dataset (http://www.resolve-whfg.appspot.com/list/Human/) and "wound healing RT2 profiler PCR array" (Qiagen). Wound healing associated soluble mediators were defined as the online dataset for

"cytokines in wound healing (R&D Systems)" supplemented with cytokines and other soluble mediators from the general wound healing associated genes list.

Single cell RNA-sequencing—The single cell sequencing experiment was performed using the 10X Genomics' Chromium Single Cell 3' gene expression V2 kit following the manufacturer's instruction. $CD4^+CD25^+$ T cells were freshly isolated from peripheral blood of 3 healthy donors. Cells were captured for each sample and libraries were sequenced on the Illumina Hiseq 3000 instrument. Raw reads from the 3 samples were combined and processed using 10x Genomics Cell Ranger v2.1 [60]. The result was summarized into an expression matrix with the unique molecular identifier (UMI) count for every cell and every gene. Genes expressed in < 3 genes and cells with < 200 genes detected or > 5% of the total UMI count in mitochondrial genes were removed, resulting a final matrix comprising 2,636 cells and 15,357 genes. Dropouts were imputed using DrImpute [61]. We analyzed data using the R package Seurat [62] with default parameters if not specified. Top 15 principal components were used to compute the tSNE plot. Resolution was set to 0.4 for clustering.

Methylation analysis

For CpG methylation analysis 250,000 cells from each desired population were FACS sorted. CpG methylation analysis was determined by pyrosequencing of bisulphite-modified genomic DNA. Methylation analysis was conducted by EpigenDx, as previously described by [63]. CpG methylation of *FOXP3* TSDR (ADS783FS2), *IL2RA* (ADS4564FS) and *CTLA4* (ADS3074FS2) loci shown in Supplementary Fig. 2g were evaluated.

TCRBV sequencing

For TCRBV sequencing 250,000 cells from each population were FACS sorted. Amplification and sequencing of *TCRB* CDR3 was performed by Adaptive Biotechnologies using the immunoSEQ Platform [64,65]. Analysis was performed using ImmunoSEQ analyser for spectratyping analysis and clone sharing among samples; to assess the overlap in TCR composition between populations, the Morisita–Horn similarity index [32] was calculated using R-Studio. Only productive (in frame and without included STOP codon) amino acidic (VJ) sequences were analysed; the number of both common and specific sequences for each combination of populations was used to calculate the percentage of unique and shared sequences within the different populations.

DCs generation, MLR and CD161 induction

From PBMCs, $CD14^+$ cells were isolated with CD14 microbeads (Miltenyi Biotec) and DCs generated by culturing for 5 days in X-Vivo 5% HS supplemented with 50ng/ml GM-CSF (Peprotech) and 800U/ml IL-4 (R&D). Maturation of the DCs was achieved by culturing for further 48h with 50ng/ml GM-CSF, 800U/ml IL-4, 10ng/ml of IL-1β, IL-6 (eBioscience), TNF-α (Biolegend) and 1μg/ml of PGE2 (BioVision) and LPS (Sigma-Aldrich). To assess the capacity of the DCs to produce ATRA the ALDEFLUOR kit (STEMCELL Technologies) was used to stain the cells for ALDH. Mixed lymphocyte reaction (MLR) was performed by co-culturing DCs with total T_{reg} cells for 5 days in the presence or absence of 1μM pan RAR inverse agonist (BMS493, Tocris Bioscience).

RARA ChIP-qPCR

JASPAR [66] was used to scan the sequences of both *KLRB1* and *CCR9* gene loci (± 5kb from gene body) for predicted binding sites of ATRA. 15×10^6 cells were cultured for 4h in X-Vivo, not supplemented with human serum, in the presence or absence of 2μM of ATRA (Sigma-Aldrich). RARA ChIP-qPCR was then performed. Briefly, cells were fixed with 16% Formaldehyde (ThermoFisher) and harvested in PBS containing protease inhibitors Aprotinin (MP biochemicals), Leupeptin (Bachem), both at 1μg/mL and 1mM Phenylmethylsulfonyl fluoride (PMSF, Sigma). Frozen cell pellets were lyzed in SDS lysis buffer containing protease inhibitors and DNA sheared into lengths of 0.2–1Kbp using a Branson sonicator (11% power amplitude). Samples were resuspended in 2ml of ChIP dilution buffer (0.01% SDS, 1.1% Triton X-100 (Sigma), 1.2mM EDTA, 16.7mM Tris HCl pH8.1, 167mM NaCl in dH_2O) containing protease inhibitors; 100μl of samples were taken as input DNA and stored for downstream qPCR. To reduce non-specific binding, samples were pre-cleared by incubation with salmon sperm DNA/protein A agarose-50% slurry (EMD Millipore). Chromatin immunoprecipitations (ChIPs) were carried out using 10μl/IP of RARA polyclonal antibody (Diagenode C15310155) and salmon sperm DNA/protein A agarose- 50% slurry. Slurry was then serially washed with Low salt wash buffer (0.1% SDS, 1% Triton X-100, 2mM EDTA, 20mM Tris HCl pH 8.1, 150mM NaCl in dH_2O) followed by High salt wash buffer (0.1% SDS, 1% Triton X-100, 2mM EDTA, 20mM Tris HCl pH 8.1, 500mM NaCl in dH_2O), LiCl wash buffer (0.25M LiCl (Sigma), 1% NP40 (ThermoFisher), 1% deoxycholate (ThermoFisher), 1mM EDTA, 10mM Tris HCl pH 8.1 in dH_2O) and finally twice with TE buffer pH 8 before elution form the beads with elution buffer (1% SDS, 0.1M $NaHCO_3$). Cross-linking was reversed with 5M NaCl/ml and heating to 65°C for 4 hours; dissociated transcription factors and antibodies were digested by adding 0.5M EDTA, 1M Tris HCl (pH 6.5) and 20mg/ml Proteinase K (ThermoFisher) followed by overnight incubation at 55°C. DNA was precipitated with isopropanol and re-dissolved in dH_2O before purification with MinElute PCR Purification Kit (QIAGEN). Primers for *KLRB1* (forward: GTCCCCACCCACATACACTT; reverse: AGAACAAATGAGCCTCCCAGA) and *CCR9* (forward: AGTTTCCCCTTATCCCAGCA; reverse: CAGCTACCCGATAACAACACG) were designed and used for quantification by qPCR. Percentage of input, normalising the signal obtained from the ChIP against the input sample, was calculated.

Cytokine secretion measurement

To evaluate the cytokine production of the different populations of T_{reg} cells after activation, 10^6 naive, memory and $CD161^+$ T_{reg} cells were FACS sorted and activated for 3 days with 1:1 ratio of αCD3αCD28 Dynabeads and 100U/ml of IL-2. Cytokine protein levels were measured in the supernatant by either $T_H1/T_H2/T_H17$ Cytometric Bead Array (CBA, BD) or LEGENDplex Human T helper Cytokine panel (Biolegend). To evaluate the effect of CD161 crosslinking on cytokine production 100,000 cells were stimulated for 3 days with ratio 1:1 microbeads coated with either αCD3αCD28IgG2 or αCD3αCD28αCD161 (T Cell Activation/Expansion Kit, Miltenyi Biotec, as previously described [25]) and protein levels measured in the supernatant by LEGENDplex Human T helper Cytokine panel (Biolegend).

IL-17 capture assay

10^6 $CD161^+$ T_{reg} cells were FACS sorted and then stimulated with PMA and Ionomycin for 5h. IL-17 producing $CD161^+$ T_{reg} cells were then labelled using the IL-17 Secretion Assay Kit (Miltenyi Biotec) according to manufacturer's instructions and then FACS sorted into IL-17 producing and non-producing cells. Cells were rested overnight and a standard suppression assay, including naive and memory T_{reg} cells as controls, performed. Simultaneous staining of surface and intracellular IL-17 was carried out on 10^6 $CD4^+$ T cells by incubating cells for an extra 2 hours in PMA/Io with supplementation of BD GolgiPlug, before washing and staining with surface IL-17 detection antibody (IL-17 Secretion Assay Kit, Miltenyi Biotec). Following extracellular staining and fixation/permeabilization, intracellular staining was then performed with a second αIL-17 antibody conjugated with a different fluorochrome. To validate the specificity of the double staining, staining with the antibody for intracellular IL-17 was also performed on cells without fixation/ permeabilization step, but after surface staining with IL-17 Detection antibody; lack of double positive cells in the control sample demonstrated that the staining for intracellular IL-17 was specific.

In vitro wound healing assay

The human intestinal cell line Caco-2 (clone HTB-37) was obtained from ECACC (European Collection of Cell Cultures, Health Protection Agency Culture Collection, Salisbury, UK) and grown in DMEM supplemented with 10% FBS (both from GIBCO) and 1% MEM Non-essential Amino Acid (NEAA, Sigma-Aldrich). Cells were routinely tested for contamination by mycoplasma. 250,000 Caco-2 cells were seeded into CytoSelect 24-Well Wound Healing Assay plates (Cell Biolabs) and grown until confluence for 7 days. Sorted memory and $CD161^+$ T_{reg} cells were stimulated for 3 days with 1:1 ratio of αCD3αCD28 Dynabeads and 100U/ml of IL-2 in complete RPMI (GIBCO) with 10% v/v HS and supernatant collected. Supernatant from the cells was then diluted 1:4 with fresh DMEM 10% FBS 1% NEAA and added to the Caco-2 cells, after insert removal. As negative control RPMI 10% HS diluted with 1:4 with DMEM 10% FBS 1% NEAA was used. Time-lapse image capture was recorded using Biostation CT (Nikon) over a period of 120h. Percentage of open wound was calculated using the "wound-healing" tool on NIS Elements Advanced Research Microscope Imaging Software (Nikon). For evaluation of the effect of cytokine blocking on wound healing either IgG1a (5μg/ml) together with IgG2b Isotype (5μg/ml), αIL-17 (5μg/ml), αIL-22 (5μg/ml), αIL-4 (5μg/ml), αIL-10R (10μg/ml), αIFNγ (5μg/ml), αIL-17 (5μg/ml) together with αIL-22 (5μg/ml) or αIL-10R (10μg/ml) together with αIL-4 (5μg/ml; all antibodies from R&D systems) were added to the wound healing assay; image capture was recorded at start and at 120h post culture.

Patient biopsies

Six consecutive patients who attended the endoscopy department at King's College Hospital (London, UK) for a colonoscopy required in the context of their routine clinical care were consented for the study (REC 15/LO/1998). Three patients were recruited with an established diagnosis of Crohn's disease (CD), based on conventional clinical criteria, and three without any history of chronic inflammatory bowel disease (IBD), but with

gastrointestinal symptoms or anemia that required investigation; these latter patients were then considered as “healthy individuals” with no diagnosis of CD. Peripheral blood was collected in EDTA tubes on the day of attendance to endoscopy and prior to colonoscopy. During colonoscopy 2mm biopsies were collected from inflamed sites in patients with CD or randomly for those without a diagnosis of IBD. Endoscopic findings of inflammation and/ or normal macroscopic appearances were confirmed by histopathology.

PBMC were isolated following standard isolation protocol and colonic Lamina Propria Mononuclear cells (cLPMC) were isolated after digestion of the colonic tissue as previously described [67]. Both PBMC and cLPMC were then stained for CD45, CD3, CD8, CD4, CD25, CD127, CD45RA and CD161. Total $CD4^+$ T cells were initially defined as $CD45^+CD3^+CD8\text{-}CD4^+$ and T_{reg} cells subpopulations were then selected following standard gating strategy, as previously described. T_{reg} cell populations were then compared in matched peripheral blood to colonic biopsy samples of healthy individuals and those with IBD.

Severe xeno-graft-versus-host-disease (GvHD) model

NOD/scid/IL-2R$\gamma^{-/-}$ (NOD.cg-Prkdc^{scid}Il2rg^{tm1Wjl}/SzJ) mice (NSG; The Jackson Laboratory) were used between 8–10 weeks of age. Animals were bred and maintained in the Biological Services Unit of King’s College London. All mice were kept under specific-pathogen-free conditions, and procedures were conducted in accordance with institutional guidelines (PPL70/7302) and the Home Office Animals Scientific Procedures Act (1986). Sorted Memory and $CD161^+$ T_{reg} cells were cultured in X-Vivo 15 with Gentamycin and PR (Lonza) supplemented with 5% human AB serum (HS, Biosera), 1,000 IU/ml of IL-2 (Proleukin, Novartis) and stimulated with Dynabeads Human T-Activator CD3/CD28 (GIBCO) at a 1:1 ratio for 2–3 rounds of expansion (10–14 days each). After the last round of expansion, beads were removed and the cells were rested for 2 days before injection into the mice. Human PBMCs (10×10^6) depleted of $CD25^+$ cells were injected intravenously to induce xeno-GvHD with or without *in vitro* –expanded Memory or $CD161^+$ T_{reg} cells (5×10^6) at a 2:1 PBMC : T_{reg} cells ratio. Mice injected with PBS alone were used as negative control. Mice were monitored for symptoms of xeno-GvHD over time and experiment was carried on until either a clinical score greater than 6 or a weight loss greater than 15% from the initial weight was reached. Clinical GvHD score was calculated by applying a modified scoring system (adapted from [68]: individual mice received a score of 0 to 2 for each criteria.

Grade 0 - <5% weight loss, normal posture, activity, fur texture and skin integrity;

Grade 1 – weight loss >5% to <10%, hunched posture only at rest, mild to moderately decreased activity, mild to moderate fur ruffling, scaling of paws/tail;

Grade 2 - >10% weight loss, severe hunching of posture impairing movement, severe ruffled fur/poor grooming, obvious areas of denuded skin.

Lentiviral preparation

Lentivirus was prepared by transfecting HEK293T cells (ATCC CRL-11268) and expanded in in DMEM 10% FCS and 1% PSG; cells were routinely tested for contamination by mycoplasma. 10^6 HEK293T cells were plated in DMEM 10% FCS and 1% PSG and transfected with 15μg of psPAX2 (Addgene), 5 μg of pMD2.G (Addgene) and 20μg of either Control or Bach2-expressing pLVX-EF1α-IRES-ZzGreen plasmids (Clonetech). The transfection mix was then added to an equal volume of $CaCl_2$ 0.5M. The resulting solution was added dropwise to an equal volume of 2x HEPES buffered saline (HBS; Fluka, Sigma-Aldrich Company Ltd., Dorset, England) to precipitate the DNA. After an incubation of 30 minutes at room temperature, the prepared solution was added evenly, drop wise, to the cells and the plate was incubated at 37°C overnight. Two collections of supernatant containing viral particles were performed at day 3 and 4 post transfection and concentration was performed by addition of PEG-it Virus concentration solution (SBI, System Bioscience, Mountain View, U.S.A) following manufacturer's instructions. After allowing 48 hours for virus precipitation, the solution containing the viral particles was spun at 1500g for 30mins at 4°C to obtain a viral pellet that was resuspended in 300μl of cold medium and stored at −80°C until used.

CD161$^+$ T_{reg} cells transduction

Sorted CD161$^+$ T_{reg} cells were stimulated for 3 days with anti-CD3+CD28 dynabeads (1:1 cell to bead ratio) in RPMI 10% HS supplemented with 100U/ml of IL-2. Cells were then counted, washed and resuspended at 10^6/ml. 100,000 cells were seeded in a 96 well plate and left overnight at 37ºC; the following day 1X Transdux and Max Enhancer (TransDux Max kit, SBI) were added to each well in the presence or absence of 10μl of Control or Bach2 lentivirus. 3 days post addition of the virus anti-CD3+CD28 dynabeads were magnetically removed, cells fed with fresh medium and left at 37ºC for a further 3 days. At the end of the transduction protocol, cells were counted, washed and resuspended at 10^6/ml and stimulated for another 3 days with anti-CD3+CD28 dynabeads (1:1 cell to bead ratio) in RPMI 10% HS supplemented with 100U/ml of IL-2. Supernatant was then collected and cytokine production was measured.

CD161$^+$ T_{reg} cells transfection

Sorted CD161$^+$ T_{reg} cells were stimulated for 3 days with anti-CD3+CD28 dynabeads (1:1 cell to bead ratio) in RPMI 10% HS supplemented with 100U/ml of IL-2. Cells were then counted, washed and resuspended at 2×10^6/ml. 100,000 cells were then seeded in a 96 well plate and transfected with either All star Negative Control siRNA or HS_RORC_7 Flexitube siRNA (both from Qiagen) following manufacturer's instruction; untransfected cells were used as baseline control. Cells were then cultured for 3 days at 37ºC; supernatant was then collected and cytokine production measured.

ATAC-Seq

ATAC-seq was performed according to published protocol [69] with minor modification as described in [70]. Paired-end libraries (50 cycles) were prepared according to ATAC-seq protocol (see above) with three biological replicates (i.e. cells from 3 different individuals)

for each library. The sequencing was performed using Illumina 2000. To obtain the open chromatin regions, reads were aligned to hg19 using Bowtie v2.2.9 [71] with parameters [--maxins 175 --no-discordant --no-mixed]. Properly paired and uniquely mapped alignments were extracted. The open chromatin regions were identified using Homer findPeaks tool [72] with parameters [-region -size 500 -minDist 50 -tbp 0]. All the open chromatin peaks were merged using bedtools [73] to obtain a set of all potential peaks. For each replicate, the differential set of open chromatin regions for each pair of samples (i.e. memory vs naive, memory vs CD161, naive v CD161) were extracted using homer getDifferentialPeaks with parameter –F 2 and the set of all potential peaks. For each pair of samples, the common peaks among three replicates were extracted using bedtools multiinter. All the common differential open chromatin regions were merged using bedtools and displayed using seqMINER [74] with three clusters. To identify motifs that are enriched in each cluster, we used homer findMotifsGenome on all known motifs with parameter [-size given].

Data analysis and statistical tools

Statistical analysis was carried out using GraphPad Prism 7 (GraphPad software Inc., USA). All measures of variance were expressed as mean ± standard error of the mean (SEM) and for data comparison t-test, one- or two-way RM ANOVA were used as indicated. All statistical tests were two-sided and data were considered statistically significant with $p<0.05$, $p<0.01$, $p<0.001$ or $p<0.0001$ and represented in figures as indicated. Hierarchical clustering of SPADE data was carried out using cytoClustR, available at https://github.com/kordastilab/cytoClustR. ROC curves were constructed in GraphPad Prism v7 (GraphPad software Inc) using the dataset from Haberman *et al.*, 2014 (GSE57945) as a training set, taking inflamed versus uninflamed Crohn's disease and healthy donor tissues as defined by the investigators. Test datasets were sourced from Noble *et al.*, 2010 (GSE20881) and Häsler *et al.,* 2016 [75], classifying samples as either normal versus any inflammation (Noble *et al.*, 2010) or non-inflamed versus inflamed as defined by the investigators (Häsler *et al.,* 2016). The data generated for this study have been deposited at the Gene Expression Omnibus (GEO) under accession code GSE119375.

Supplementary Material

Refer to Web version on PubMed Central for supplementary material.

Acknowledgements:

The authors wish to thank patients that contributed samples towards this study. This work was supported by the Wellcome Trust (grant 097261/Z/11/Z to B. Afzali and WT101159 to N. Powell), the Crohn's & Colitis Foundation of America (grant CCFA #3765 – CCFA genetics initiative to A. Laurence), British Heart Foundation (grant RG/13/12/30395 to G. Lombardi), institutional startup fund from Purdue university and National Heart, Lung, and Blood Institute (grant 5K22HL125593–02 to M. Kazemian). Research was also supported by the National Institute for Health Research (NIHR) Biomedical Research Centre at Guy's and St Thomas' NHS Foundation Trust and King's College London. The views expressed are those of the author(s) and not necessarily those of the NHS, the NIHR or the Department of Health. This research was supported [in part] by the Intramural Research Programs of the National Institute of Arthritis and Musculoskeletal and Skin Diseases, the National Institute of Diabetes and Digestive and Kidney Diseases and the National Heart, Lung and Blood Institute of the National Institutes of Health. We thank John O'Shea (National Institutes of Health) for his support and for providing access to ATAC-seq, the National Heart, Lung and Blood Institute DNA Sequencing and Genomics Core for performing single cell sequencing experiment and acknowledge the assistance of Matt Arno (Genomics centre, King's College London) with gene expression microarray studies as well as Suanne Heck and Richard Ellis (Biomedical research centre

flow core facility, King's College London) for CyTOF data acquisition. In addition, the authors thank Ewy Mathé (Ohio State University) for critically reading the manuscript.

References

1. Edozie FC et al. Regulatory T-cell therapy in the induction of transplant tolerance: the issue of subpopulations. Transplantation 98, 370–379 (2014). [PubMed: 24933458]
2. Sakaguchi S, Wing K, Onishi Y, Prieto-Martin P & Yamaguchi T Regulatory T cells: how do they suppress immune responses? Int Immunol 21, 1105–1111 (2009). [PubMed: 19737784]
3. Roychoudhuri R et al. BACH2 represses effector programs to stabilize T(reg)-mediated immune homeostasis. Nature 498, 506–510 (2013). [PubMed: 23728300]
4. Yadav M et al. Neuropilin-1 distinguishes natural and inducible regulatory T cells among regulatory T cell subsets in vivo. J Exp Med 209, 1713–22–S1–19 (2012). [PubMed: 22966003]
5. Thornton AM et al. Expression of Helios, an Ikaros transcription factor family member, differentiates thymic-derived from peripherally induced Foxp3+ T regulatory cells. J Immunol 184, 3433–3441 (2010). [PubMed: 20181882]
6. Floess S et al. Epigenetic control of the foxp3 locus in regulatory T cells. PLoS Biol 5, e38 (2007). [PubMed: 17298177]
7. Ohkura N et al. T Cell Receptor Stimulation-Induced Epigenetic Changes and Foxp3 Expression Are Independent and Complementary Events Required for Treg Cell Development. Immunity 37, 785–799 (2012). [PubMed: 23123060]
8. Polansky JK et al. DNA methylation controls Foxp3 gene expression. Eur J Immunol 38, 1654–1663 (2008). [PubMed: 18493985]
9. Shih H-Y et al. Transcriptional and epigenetic networks of helper T and innate lymphoid cells. Immunol Rev 261, 23–49 (2014). [PubMed: 25123275]
10. Oldenhove G et al. Decrease of Foxp3+ Treg cell number and acquisition of effector cell phenotype during lethal infection. Immunity 31, 772–786 (2009). [PubMed: 19896394]
11. Chaudhry A et al. CD4+ Regulatory T Cells Control TH17 Responses in a Stat3-Dependent Manner. Science 326, 986–991 (2009). [PubMed: 19797626]
12. Zheng Y et al. Regulatory T-cell suppressor program co-opts transcription factor IRF4 to control TH2 responses. Nature 458, 351–356 (2009). [PubMed: 19182775]
13. Koch MA et al. The transcription factor T-bet controls regulatory T cell homeostasis and function during type 1 inflammation. Nat Immunol 10, 595–602 (2009). [PubMed: 19412181]
14. Wohlfert EA et al. GATA3 controls Foxp3$^+$ regulatory T cell fate during inflammation in mice. J Clin Invest 121, 4503–4515 (2011). [PubMed: 21965331]
15. Yu F, Sharma S, Edwards J, Feigenbaum L & Zhu J Dynamic expression of transcription factors T-bet and GATA-3 by regulatory T cells maintains immunotolerance. Nat Immunol 16, 197–206 (2015). [PubMed: 25501630]
16. Kordasti S et al. Deep phenotyping of Tregs identifies an immune signature for idiopathic aplastic anemia and predicts response to treatment. 128, 1193–1205 (2016).
17. Miyara M et al. Functional delineation and differentiation dynamics of human CD4+ T cells expressing the FoxP3 transcription factor. Immunity 30, 899–911 (2009). [PubMed: 19464196]
18. Booth NJ et al. Different proliferative potential and migratory characteristics of human CD4+ regulatory T cells that express either CD45RA or CD45RO. J Immunol 184, 4317–4326 (2010). [PubMed: 20231690]
19. Maloy KJ & Powrie F Intestinal homeostasis and its breakdown in inflammatory bowel disease. Nature 474, 298–306 (2011). [PubMed: 21677746]
20. Povoleri GAM et al. Thymic versus induced regulatory T cells - who regulates the regulators? Front. Immunol 4, 169 (2013). [PubMed: 23818888]
21. Maloy KJ et al. CD4+CD25+ T(R) cells suppress innate immune pathology through cytokine-dependent mechanisms. J Exp Med 197, 111–119 (2003). [PubMed: 12515818]
22. Maul J et al. Peripheral and intestinal regulatory CD4+ CD25(high) T cells in inflammatory bowel disease. Gastroenterology 128, 1868–1878 (2005). [PubMed: 15940622]

23. Afzali B et al. CD161 expression characterizes a subpopulation of human regulatory T cells that produces IL-17 in a STAT3-dependent manner. Eur J Immunol 43, 2043–2054 (2013). [PubMed: 23677517]
24. Lanier LL, Chang C & Phillips JH Human NKR-P1A. A disulfide-linked homodimer of the C-type lectin superfamily expressed by a subset of NK and T lymphocytes. J Immunol 153, 2417–2428 (1994). [PubMed: 8077657]
25. Fergusson JR et al. CD161 Defines a Transcriptional and Functional Phenotype across Distinct Human T Cell Lineages. Cell Rep 9, 1075–1088 (2014). [PubMed: 25437561]
26. Cosmi L et al. Human interleukin 17-producing cells originate from a CD161+CD4+ T cell precursor. J Exp Med 205, 1903–1916 (2008). [PubMed: 18663128]
27. Germain C et al. Induction of lectin-like transcript 1 (LLT1) protein cell surface expression by pathogens and interferon-γ contributes to modulate immune responses. J Biol Chem 286, 37964–37975 (2011). [PubMed: 21930700]
28. Wolfkamp SCS et al. Single nucleotide polymorphisms in C-type lectin genes, clustered in the IBD2 and IBD6 susceptibility loci, may play a role in the pathogenesis of inflammatory bowel diseases. Eur J Gastroenterol Hepatol 24, 965–970 (2012). [PubMed: 22664939]
29. Diggins KE, Ferrell PB & Irish JM Methods for discovery and characterization of cell subsets in high dimensional mass cytometry data. Methods 82, 55–63 (2015). [PubMed: 25979346]
30. Qiu P et al. Extracting a cellular hierarchy from high-dimensional cytometry data with SPADE. Nat Biotechnol 29, 886–891 (2011). [PubMed: 21964415]
31. Thomas SY et al. CD1d-restricted NKT cells express a chemokine receptor profile indicative of Th1-type inflammatory homing cells. J Immunol 171, 2571–2580 (2003). [PubMed: 12928408]
32. Venturi V et al. Method for assessing the similarity between subsets of the T cell receptor repertoire. J Immunol Methods 329, 67–80 (2008). [PubMed: 18001765]
33. Ferraro A et al. Interindividual variation in human T regulatory cells. Proc Natl Acad Sci 111, E1111–20 (2014). [PubMed: 24610777]
34. Kim YC et al. Oligodeoxynucleotides stabilize Helios-expressing Foxp3+ human T regulatory cells during in vitro expansion. Blood 119, 2810–2818 (2012). [PubMed: 22294730]
35. Scotta C et al. Differential effects of rapamycin and retinoic acid on expansion, stability and suppressive qualities of human CD4(+)CD25(+)FOXP3(+) T regulatory cell subpopulations. Haematologica 98, 1291–1299 (2013). [PubMed: 23242600]
36. Afzali B et al. Comparison of regulatory T cells in hemodialysis patients and healthy controls: implications for cell therapy in transplantation. Clin J Am Soc Nephrol 8, 1396–1405 (2013). [PubMed: 23580782]
37. Thornton AM & Shevach EM CD4+CD25+ immunoregulatory T cells suppress polyclonal T cell activation in vitro by inhibiting interleukin 2 production. J Exp Med 188, 287–296 (1998). [PubMed: 9670041]
38. Cao X et al. Granzyme B and Perforin Are Important for Regulatory T Cell-Mediated Suppression of Tumor Clearance. Immunity 27, 635–646 (2007). [PubMed: 17919943]
39. Rosen DB et al. Functional consequences of interactions between human NKR-P1A and its ligand LLT1 expressed on activated dendritic cells and B cells. J Immunol 180, 6508–6517 (2008). [PubMed: 18453569]
40. Kitoh A et al. Indispensable Role of the Runx1-Cbfβ Transcription Complex for In Vivo-Suppressive Function of FoxP3+ Regulatory T Cells. Immunity 31, 609–620 (2009). [PubMed: 19800266]
41. Ciofani M et al. A validated regulatory network for Th17 cell specification. Cell 151, 289–303 (2012). [PubMed: 23021777]
42. Afzali B et al. BACH2 immunodeficiency illustrates an association between super-enhancers and haploinsufficiency. Nat Immunol 18, 813–823 (2017). [PubMed: 28530713]
43. Hong SN et al. RNA-seq Reveals Transcriptomic Differences in Inflamed and Noninflamed Intestinal Mucosa of Crohn's Disease Patients Compared with Normal Mucosa of Healthy Controls. Inflamm. Bowel Dis 23, 1098–1108 (2017). [PubMed: 28613228]
44. Sefik E et al. MUCOSAL IMMUNOLOGY. Individual intestinal symbionts induce a distinct population of RORγ$^+$ regulatory T cells. Science 349, 993–997 (2015). [PubMed: 26272906]

45. Kim B-S et al. Generation of RORγt+ Antigen-Specific T Regulatory 17 Cells from Foxp3+ Precursors in Autoimmunity. Cell Rep 21, 195–207 (2017). [PubMed: 28978473]
46. Hovhannisyan Z, Treatman J, Littman DR & Mayer L Characterization of interleukin-17-producing regulatory T cells in inflamed intestinal mucosa from patients with inflammatory bowel diseases. Gastroenterology 140, 957–965 (2011). [PubMed: 21147109]
47. Blatner NR et al. Expression of RORγt marks a pathogenic regulatory T cell subset in human colon cancer. Sci Trans Med 4, 164ra159–164ra159 (2012).
48. Komatsu N et al. Pathogenic conversion of Foxp3+ T cells into TH17 cells in autoimmune arthritis. Nat Med 20, 62–68 (2014). [PubMed: 24362934]
49. Yang B-H et al. Foxp3(+) T cells expressing RORγt represent a stable regulatory T-cell effector lineage with enhanced suppressive capacity during intestinal inflammation. Mucosal Immunology 9, 444–457 (2016). [PubMed: 26307665]
50. Nosbaum A et al. Regulatory T Cells Facilitate Cutaneous Wound Healing. J Immunol 196, 2010–2014 (2016). [PubMed: 26826250]
51. O'Connor W et al. A protective function for interleukin 17A in T cell-mediated intestinal inflammation. Nat Immunol 10, 603–609 (2009). [PubMed: 19448631]
52. Hueber W et al. Secukinumab, a human anti-IL-17A monoclonal antibody, for moderate to severe Crohn's disease: unexpected results of a randomised, double-blind placebo-controlled trial. Gut 61, 1693–1700 (2012). [PubMed: 22595313]
53. Lindemans CA et al. Interleukin-22 promotes intestinal-stem-cell-mediated epithelial regeneration. Nature 528, 560–564 (2015). [PubMed: 26649819]
54. Zenewicz LA et al. Innate and adaptive interleukin-22 protects mice from inflammatory bowel disease. Immunity 29, 947–957 (2008). [PubMed: 19100701]

Experimental procedures references

55. Amir E-AD et al. viSNE enables visualization of high dimensional single-cell data and reveals phenotypic heterogeneity of leukemia. Nat Biotechnol 31, 545–552 (2013). [PubMed: 23685480]
56. Subramanian A et al. Gene set enrichment analysis: a knowledge-based approach for interpreting genome-wide expression profiles. Proc Natl Acad Sci USA 102, 15545–15550 (2005). [PubMed: 16199517]
57. Barrientos S, Stojadinovic O, Golinko MS, Brem H & Tomic-Canic M Growth factors and cytokines in wound healing. Wound Repair Regen 16, 585–601 (2008). [PubMed: 19128254]
58. Deonarine K et al. Gene expression profiling of cutaneous wound healing. J Transl Med 5, 11 (2007). [PubMed: 17313672]
59. Peake MA et al. Identification of a transcriptional signature for the wound healing continuum. Wound Repair Regen 22, 399–405 (2014). [PubMed: 24844339]
60. Zheng GXY et al. Massively parallel digital transcriptional profiling of single cells. Nat Commun 8, 14049 (2017). [PubMed: 28091601]
61. Gong W, Kwak I-Y, Pota P, Koyano-Nakagawa N & Garry DJ DrImpute: imputing dropout events in single cell RNA sequencing data. BMC Bioinformatics 19, 220 (2018). [PubMed: 29884114]
62. Butler A, Hoffman P, Smibert P, Papalexi E & Satija R Integrating single-cell transcriptomic data across different conditions, technologies, and species. Nat Biotechnol 36, 411–420 (2018). [PubMed: 29608179]
63. Zheng Y et al. Role of conserved non-coding DNA elements in the Foxp3 gene in regulatory T-cell fate. Nature 463, 808–812 (2010). [PubMed: 20072126]
64. Robins HS et al. Comprehensive assessment of T-cell receptor beta-chain diversity in alphabeta T cells. 114, 4099–4107 (2009).
65. Carlson CS et al. Using synthetic templates to design an unbiased multiplex PCR assay. Nat Commun 4, 2680 (2013). [PubMed: 24157944]
66. Mathelier A et al. JASPAR 2016: a major expansion and update of the open-access database of transcription factor binding profiles. Nucleic Acids Res 44, D110–5 (2016). [PubMed: 26531826]

67. Rovedatti L et al. Differential regulation of interleukin 17 and interferon gamma production in inflammatory bowel disease. Gut 58, 1629–1636 (2009). [PubMed: 19740775]

68. Cooke KR et al. An experimental model of idiopathic pneumonia syndrome after bone marrow transplantation: I. The roles of minor H antigens and endotoxin. 88, 3230–3239 (1996).

69. Buenrostro JD, Giresi PG, Zaba LC, Chang HY & Greenleaf WJ Transposition of native chromatin for fast and sensitive epigenomic profiling of open chromatin, DNA-binding proteins and nucleosome position. Nature Methods 10, 1213–1218 (2013). [PubMed: 24097267]

70. Shih H-Y et al. Developmental Acquisition of Regulomes Underlies Innate Lymphoid Cell Functionality. Cell 165, 1120–1133 (2016). [PubMed: 27156451]

71. Langmead B & Salzberg SL Fast gapped-read alignment with Bowtie 2. Nature Methods 9, 357–359 (2012). [PubMed: 22388286]

72. Heinz S et al. Simple combinations of lineage-determining transcription factors prime cis-regulatory elements required for macrophage and B cell identities. Mol. Cell 38, 576–589 (2010). [PubMed: 20513432]

73. Quinlan AR & Hall IM BEDTools: a flexible suite of utilities for comparing genomic features. Bioinformatics 26, 841–842 (2010). [PubMed: 20110278]

74. Ye T et al. seqMINER: an integrated ChIP-seq data interpretation platform. Nucleic Acids Res 39, e35–e35 (2011). [PubMed: 21177645]

75. Häsler R et al. Uncoupling of mucosal gene regulation, mRNA splicing and adherent microbiota signatures in inflammatory bowel disease. Gut (2016). doi:10.1136/gutjnl-2016-311651.

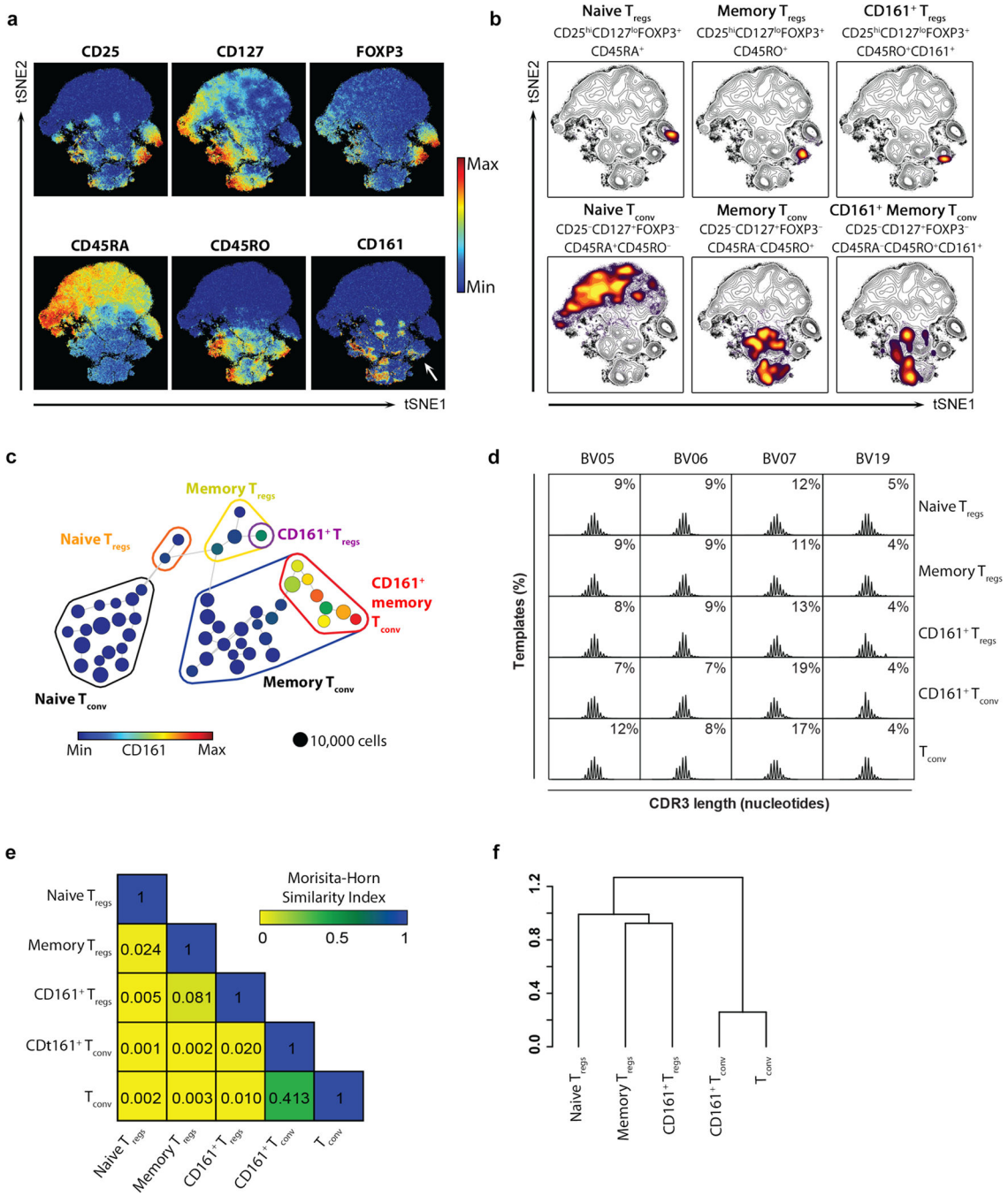

Figure 1. CD161$^+$ T_{reg} cells are a discrete population of memory T_{reg} cells.

(**a**) viSNE plots of CD4$^+$ T cells clustered using surface and intracellular markers. Shown are heatmaps for expression of indicated markers. White arrow highlights expression of CD161 within T_{reg} cells; (**b**) overlaid contour plots of T cell subsets, colored by density, to highlight sub-populations of T_{reg} cells and T_{conv}; (**c**) 2D minimum spanning tree showing population nodes of CD4$^+$ T cells. Node size represents cell number and color CD161 median intensity. Grouped together are naive (circled in orange), memory (circled in yellow) and CD161$^+$ (circled in purple) T_{reg} cells, as well as populations of naive (circled in black),

memory (circled in black) and CD161^{+} (circled in red) T_{conv}; (**a-c**) show representative data from n=3 experiments; (**d**) representative spectratype histograms from n=3 experiments showing percentage of unique CDR3 sequences (templates) versus CDR3 length for the three highest (BV05, BV06 and BV07) and one of the lowest (BV19) TCRBV families contributing to the overall TCR repertoire in the indicated populations; (**e**) average Morisita-Horn Similarity Index of total TCRVB repertoire between the T cell populations (cumulative data from n=3 experiments); and (**f**) dendrogram showing linkage distance based on the Morisita-Horn Similarity Index.

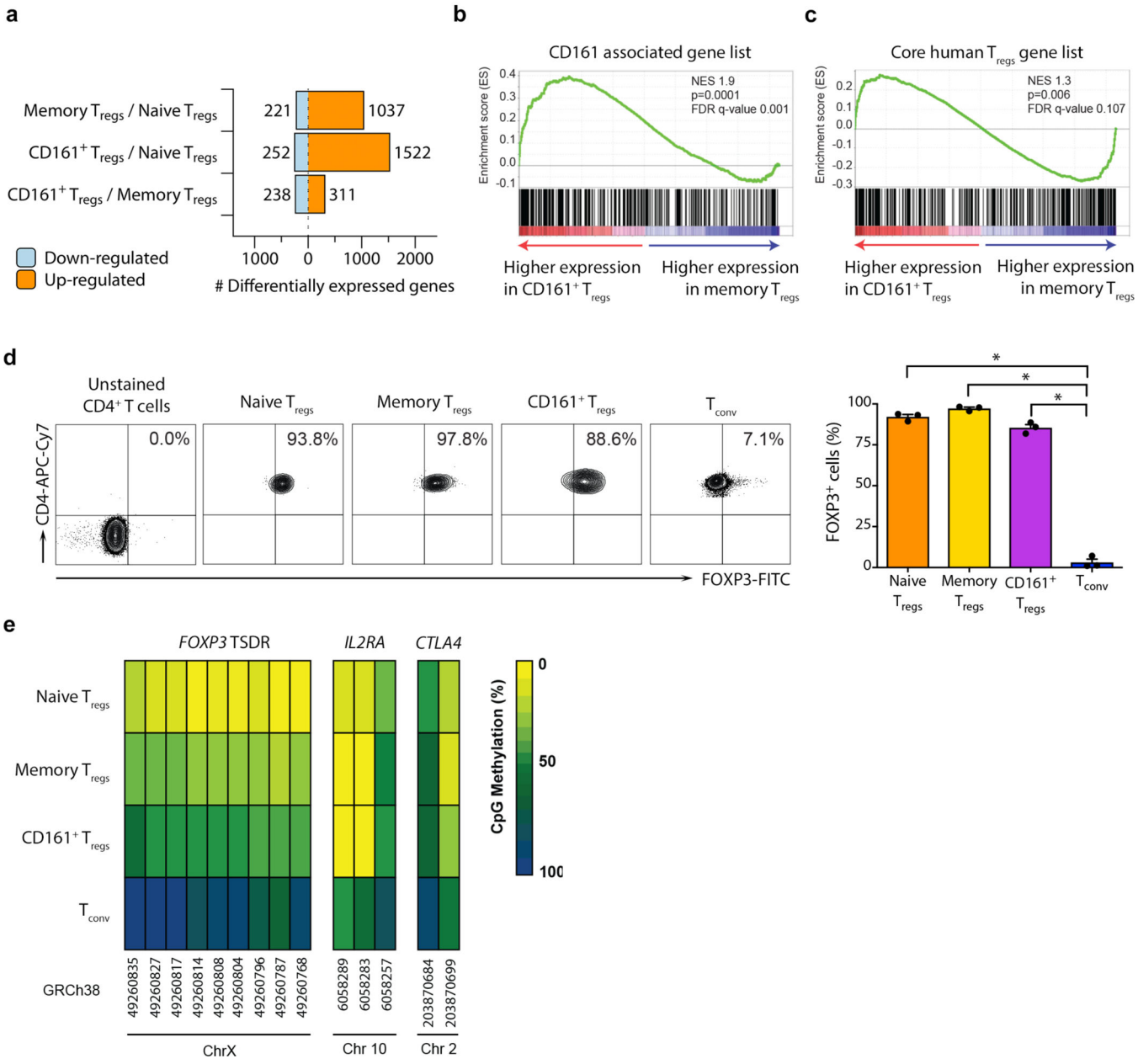

Figure 2. CD161$^+$ T$_{reg}$ cells have classical features of *bona fide* T$_{reg}$ cells.

(**a**) number of differentially expressed genes between the sub-populations of freshly isolated T$_{reg}$ cells; (**b-c**) Gene Set Enrichment Analysis (GSEA) plots for genes associated with other CD161$^+$ cells (**b**) and core human T$_{reg}$ signature genes (**c**) comparing freshly isolated memory to CD161$^+$ T$_{reg}$ cells (n=3 per group); NES = normalized enrichment score; empirical p- and multiple test adjusted q-values from GSEA are shown; (**d**) FOXP3 expression by sub-populations of T$_{reg}$ cells and T$_{conv}$, showing representative flow cytometry plots (left) and cumulative data (mean + sem; right); (**e**) mean percentage CpG methylation of conserved CpGs (with chromosomal coordinates) at the *FOXP3* TSDR,

IL2RA and *CTLA4* loci of naive, memory, $CD161^+$ T_{reg} cells and T_{conv} of 3 male donors. n=3 independent experiments in **a-e**; *p<0.0001 by one-way ANOVA.

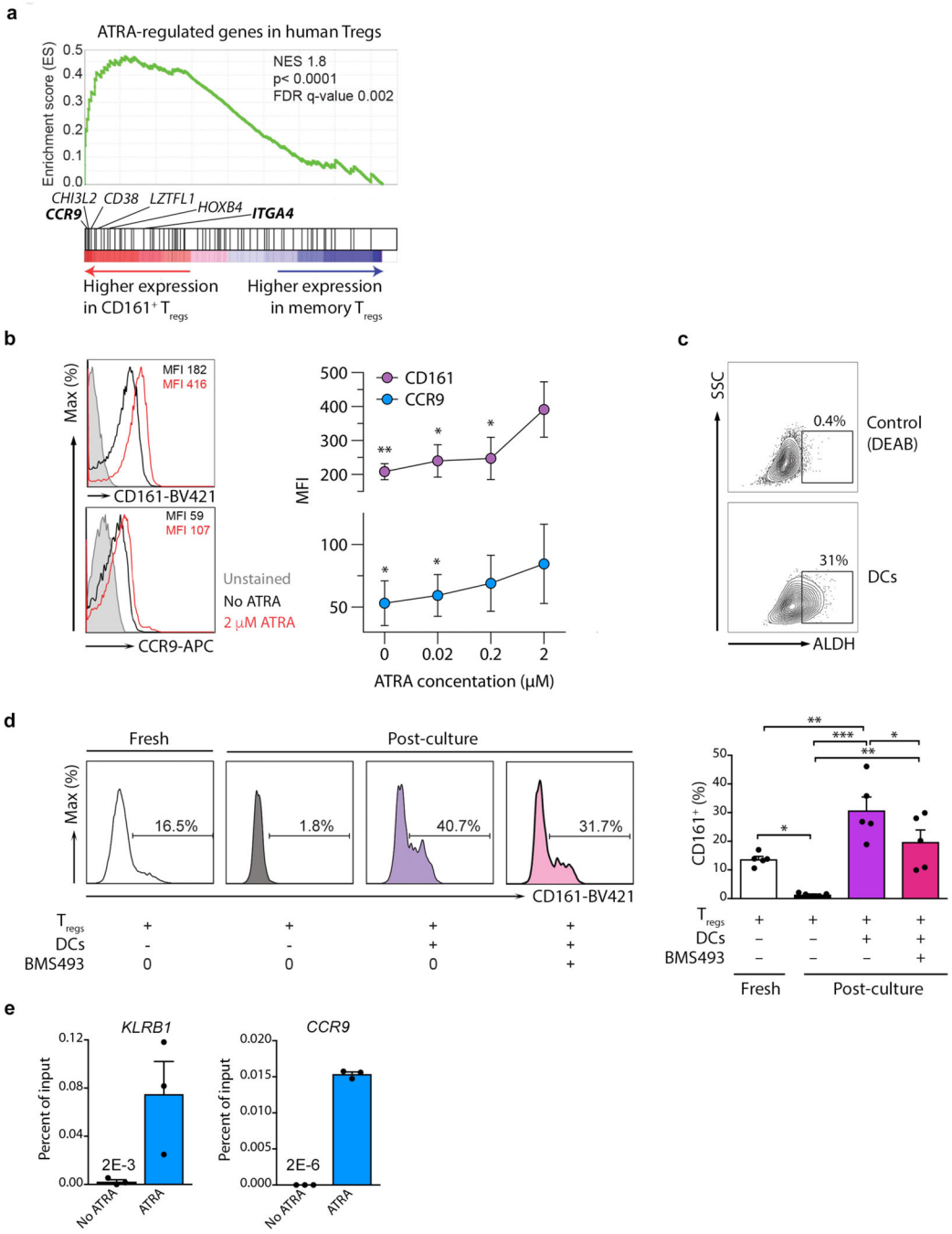

Figure 3. CD161 expression is regulated by retinoic acid.

(**a**) GSEA for ATRA-regulated genes in human T_{reg} cells comparing freshly isolated memory to $CD161^+$ T_{reg} cells. Classic ATRA-regulated genes within the leading edge of core enriched genes (see Supplementary Fig. 3a) are annotated. In bold are gut homing receptors; n=3 per group; NES = normalized enrichment score; empirical p- and multiple-test adjusted q-values from GSEA are shown; (**b**) expression of CD161 and CCR9 on T_{reg} cells cultured with and without ATRA for 2 days; shown are representative flow cytometry plots (left) and cumulative data from n=3 experiments (right); p-values indicate comparisons

with 2μM ATRA; (**c**) representative assay of ALDH activity in DCs from n=3 independent experiments; (**d**) representative flow cytometry plots (left) and cumulative data (right) from n=5 independent experiments showing CD161 expression on T_{reg} cells before (fresh) and after 5 days either with medium alone or co-culture with DCs in the presence or absence of the pan-RAR inverse agonist, BMS493; (**e**) RARA ChIP-qPCR for binding sites in *KLRB1* and *CCR9*, showing percentage of input; shown are representative examples from n=2 independent experiments. Bar charts show mean + sem throughout; *p<0.05, **p<0.01, ***p<0.001 by one-way ANOVA.

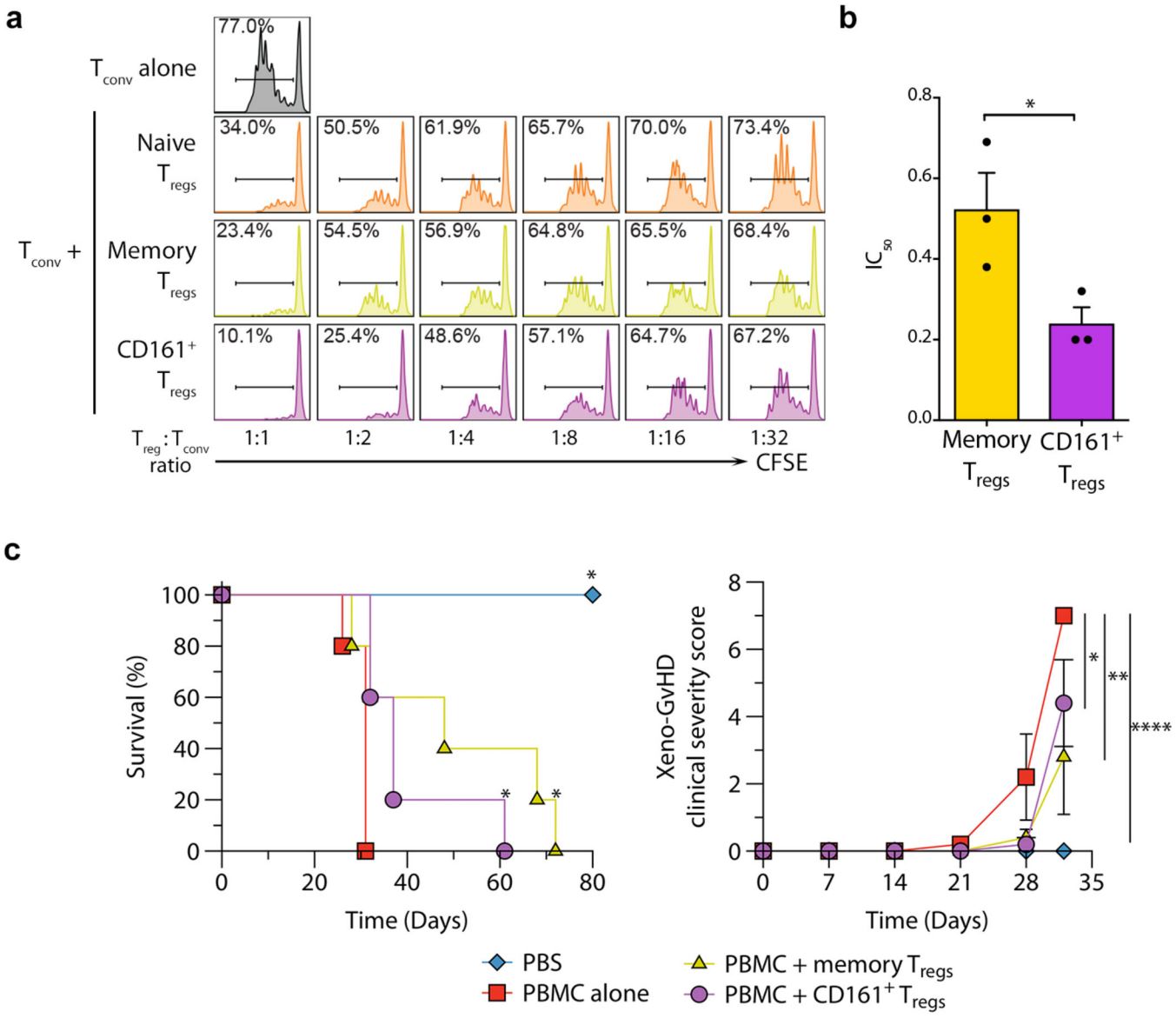

Figure 4. CD161$^+$ T_{reg} cells are regulatory both *in vitro* and *in vivo*.

(**a-b**) *In vitro* T_{reg} suppression assay showing representative CFSE dilution histograms of T_{conv} co-cultured with and without T_{reg} cells (**a**) and cumulative IC_{50} of memory and CD161$^+$ T_{reg} cells from n=3 experiments (**b**). Note that only one out of the 3 naive T_{reg} donors tested reached 50% suppression, therefore the mean IC_{50} was not calculated for the naive T_{reg} population. Bars show mean + sem. (**c**) Xeno-graft versus host disease with and without 2:1 PBMC : T_{reg} cell injection, showing survival plots (left panel; * p<0.05 compared to PBMC alone) and clinical severity (right panel). Shown is one experiment from two independent experiments carried out with n=5 mice in each group. Error bars indicate mean + sem; *p<0.05, **p<0.01, ***p<0.0001 by t-test (**b**), long-rank (Mantel-Cox) test (**c**, left) and two-way ANOVA (**c**, right).

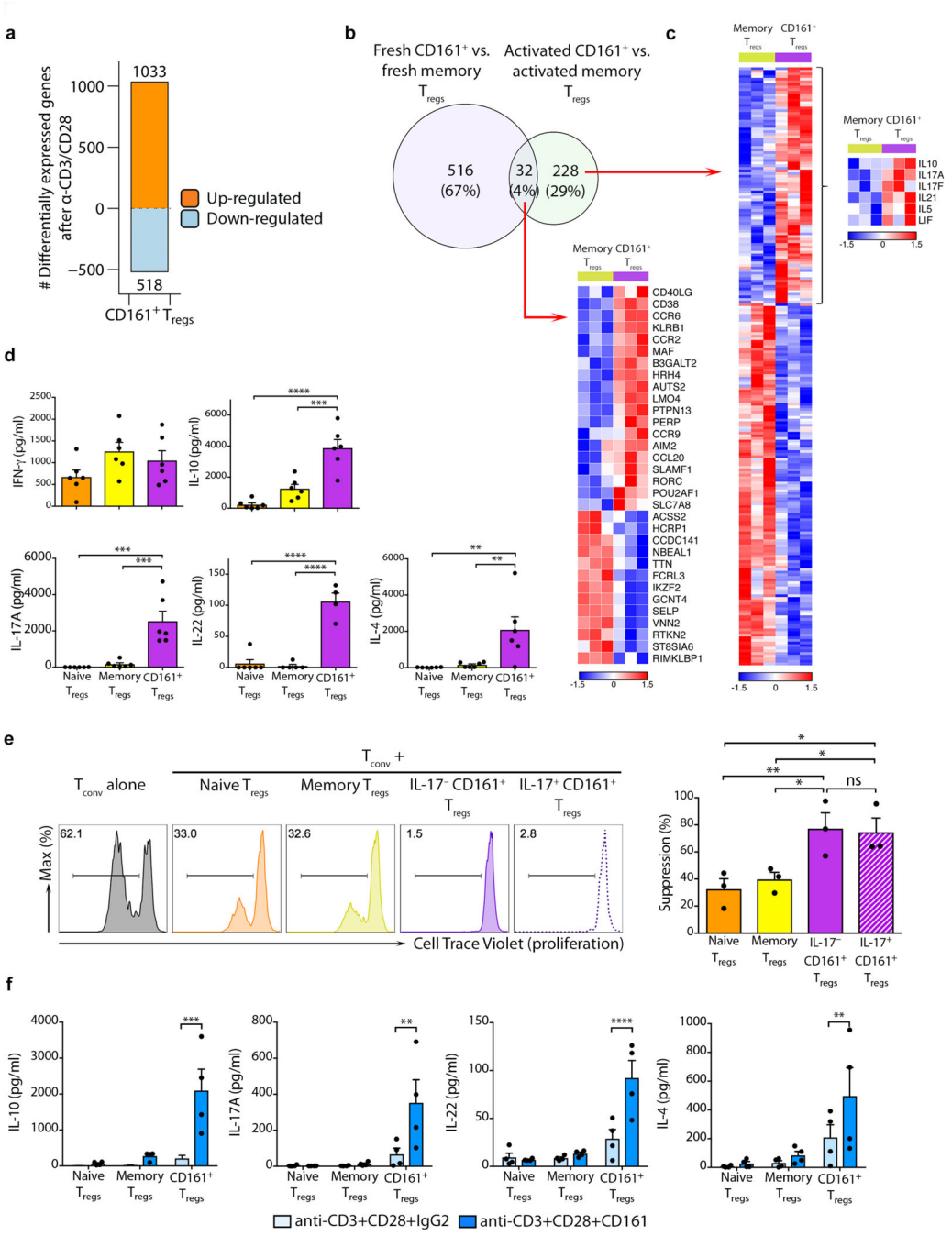

Figure 5. CD161 ligation is co-stimulatory and induces cytokine production from CD161$^+$ T$_{reg}$ cells.

(**a**) differentially expressed genes following 4h stimulation of CD161$^+$ T$_{reg}$ cells with anti-CD3/CD28; (**b**) venn diagram of transcriptional differences between freshly isolated and *in vitro* anti-CD3/CD28-activated CD161$^+$ and memory T$_{reg}$ cells; (**c**) heatmaps of differentially expressed genes common to fresh and activated cells (lower panel) and specific to the activated condition (right panel), with cytokine genes highlighted in inset. Data in **a-c** are from 3 independent experiments; (**d**) concentration (pg/ml) of stated cytokines in

supernatants of naive, memory and CD161$^+$ T_{reg} cells after 3 days of polyclonal activation with anti-CD3+CD28 (cumulative data from n=6 experiments); (**e**) suppression assay showing cell trace violet dilution in proliferating T_{conv} cultured alone or in co-culture with stated populations of T_{reg} cells (T_{reg} cell: T_{conv} ratio of 1:2). Shown are representative plots (left) and cumulative data from n=3 independent experiments (right); (**f**) concentrations of stated cytokines in supernatants of FACS-sorted CD161$^+$ T_{reg} cells stimulated for 3 days with either anti-CD3+CD28+IgG2 or anti-CD3+CD28+CD161-coated magnetic beads (cumulative data from n=4 experiments). Bar charts shown mean + sem throughout. *p<0.05, **p<0.01, ***p<0.001, ****p<0.0001 by one-way (**d-e**) and two-way ANOVA (**f**).

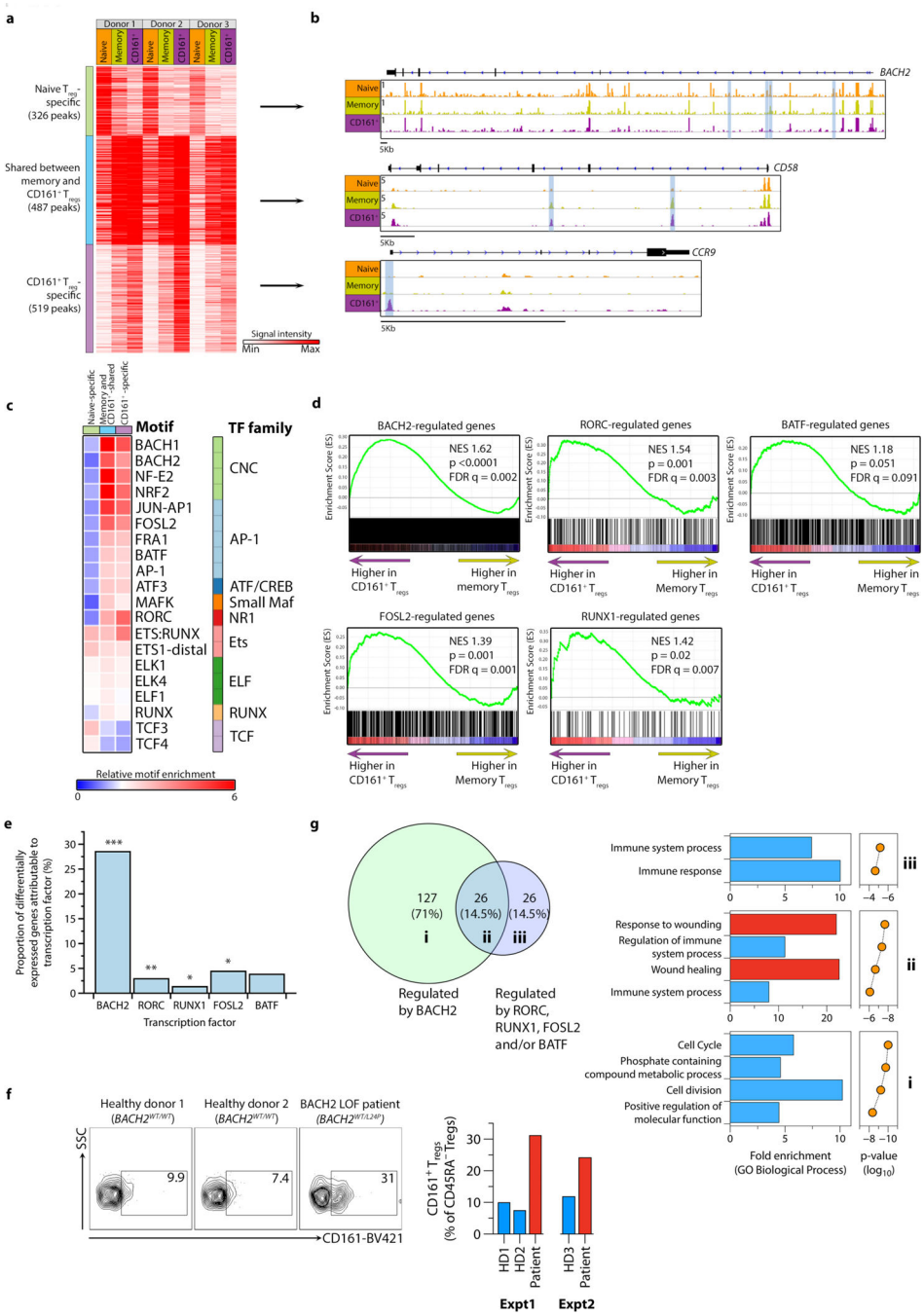

Figure 6. Genome-wide chromatin landscapes define the regulatory circuitry of CD161^{+} T$_{reg}$ cells.

(**a-b**) heatmap showing signal intensity of each ATAC peak and clustering of peaks into three groups (**a**) with representative examples of open chromatin regions (OCRs) from the three clusters (**b**) - highlighted in blue are OCRs corresponding to ATAC peaks in the heatmap; (**c**) transcription factor (TF) footprints enriched relative to background in each cluster of ATAC peaks, with corresponding TF family indicated; (**d**) GSEA plots for BACH2-, RORγt-, BATF-, FOSL2- and RUNX1-regulated genes, comparing memory to

$CD161^+$ T_{reg} cells; n=3 per group; NES = normalized enrichment score; empirical p- and multiple-test adjusted q-values from GSEA are shown; (**e**) percentage of differentially expressed genes (DEG) between $CD161^+$ and memory T_{reg} cells that can be explained by each TF; **(f)** CD161 expression on $CD4^+CD25^{hi}CD127^{lo}CD45RA^-$ T_{reg} cells of healthy age and sec-matched donors ($BACH2^{WT/WT}$) and a patient with BACH2 haploinsufficiency ($BACH2^{WT/L24P}$); shown are representative flow cytometry plots (left) and data from two independent experiments (right); (**g**) Venn diagram showing shared and unique DEGs regulated by TFs (see also Supplementary Fig. 6e) (left) and corresponding function for those DEGs (right). Data for **Fig. 6a-e** and **g** are from n=3 independent experiments. *p<0.05, **p<0.01, ***p<0.001 by Fisher exact test.

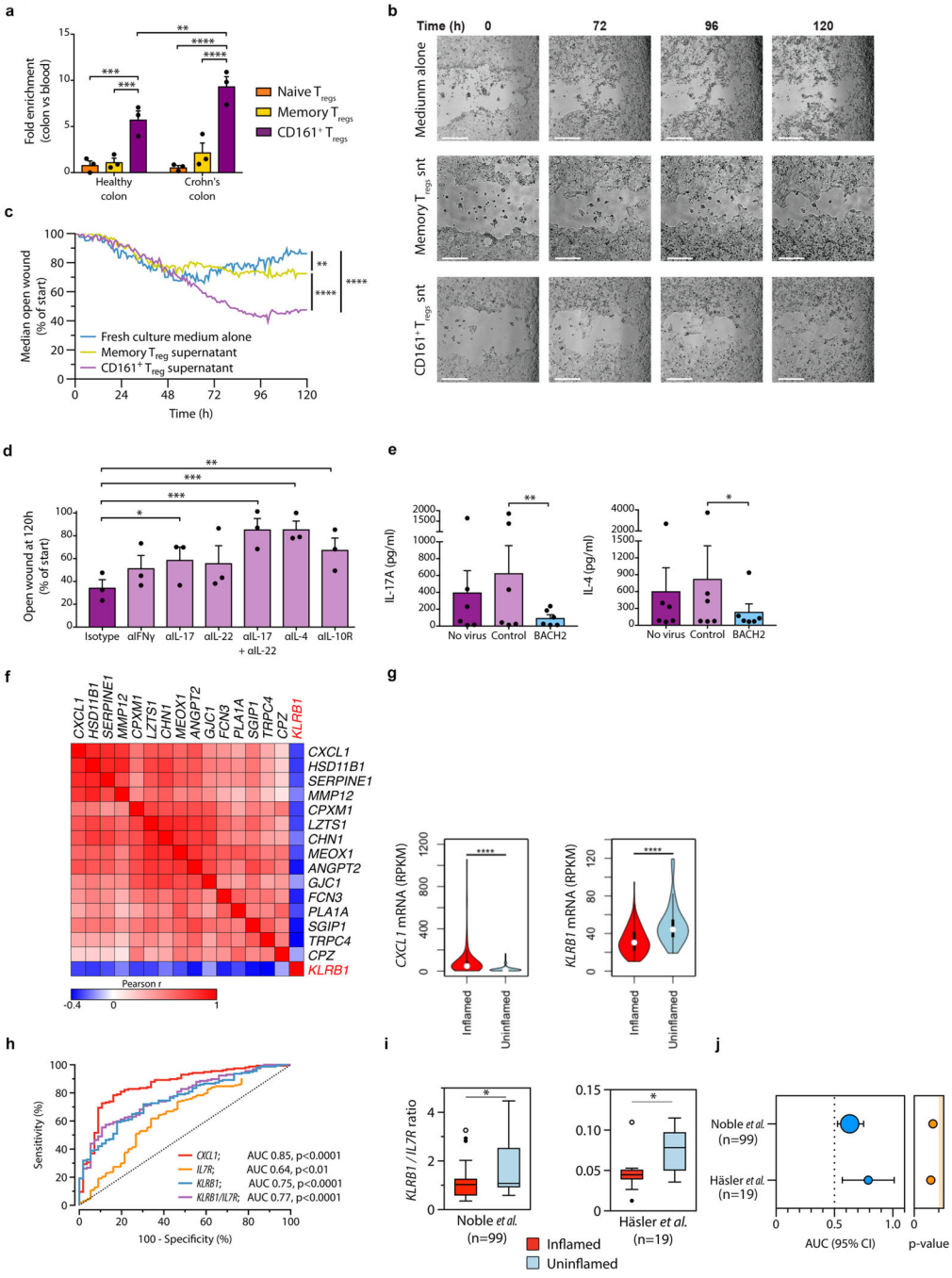

Figure 7. CD161$^+$ T$_{reg}$ cells accelerate wound healing and are associated with lower inflammation in IBD.

(**a**) enrichment of T$_{reg}$ cells sub-populations in colons relative to blood of healthy subjects and patients with Crohn's disease (CD) (n=3 paired samples per group); (**b-c**) wound healing assay showing growth of Caco-2 cells cultured with medium alone or medium supplemented with culture supernatants (snt) of activated memory or CD161$^+$ T$_{reg}$ cells; representative images captured over time (0, 72, 96 and 120h; white bars=0.5mm) (**b**) and percentage of open wound over time from n=3 experiments (**c**); (**d**) Open wound fraction at

culture end for Caco-2 cells in the presence of culture supernatants from activated CD161$^+$ T_{reg} cells with blocking antibodies to stated cytokines or isotype control; cumulative data from *n*=3 experiments. (**e**) Concentration (pg/ml) of stated cytokines in supernatants of CD161$^+$ T_{reg} cells transduced, or not, with lentivirus encoding BACH2 or control virus (cumulative data from *n*=6 experiments); (**f**) correlation matrix of indicated transcripts in bowel specimens of active CD (*n*=171); (**g**) violin plots showing distribution of *CXCL1* (left) and *KLRB1* (right) expression in inflamed (*n*=157) and uninflamed CD or non-IBD tissue biopsies (*n*=56); (**h**) receiver operating characteristic (ROC) curves showing performance of *CXCL1*, *IL7R*, *KLRB1* and *KLRB1*/*IL7R* ratio to discriminate inflamed (*n*=157) versus uninflamed CD or non-IBD tissue (*n*=56). Area under the ROC curve analyses (AUC) and their *p*-values indicated. (**i-j**) *KLRB1*/*IL7R* ratio in transcriptomes of inflamed and uninflamed sites of CD (**i**) and AUC + 95% CI of *KLRB1*/*IL7R* ROC curves to distinguish the two (**j**) from two additional, independent, datasets. Numbers of biologically independent samples (*n*) in **i** is indicated. In j, areas of circles indicate sample size. Source data for **f-h**: GSE57945; **i-j**: GSE20881 and Häsler *et al.*, 2016. Bars show mean + sem throughout; *p<0.05, **p<0.01, ***p<0.001, ****p<0.0001 by one-way (**d-e**) and two-way ANOVA (**a** and **c**), t-test (**g** and **i**) and AUC analysis (**h** and **j**).